Simulating sediment supply from the Congo watershed over the last 155 ka

Stéphane Molliex, Albert Kettner, Dimitri Laurent, Laurence Droz, Tania Marsset, Alain Laraque, Marina Rabineau, Guy Moukandi N'Kaya

Quaternary Science Reviews
January 2019, Volume 203 Pages 38-55
https://doi.org/10.1016/j.quascirev.2018.11.001
https://archimer.ifremer.fr/doc/00467/57897/

Simulating sediment supply from the Congo watershed over the last 155 ka

Molliex Stéphane [1, *], Kettner Albert J. [2], Laurent Dimitri [3], Droz Laurence [6], Marsset Tania [3], Laraque Alain [4], Rabineau Marina [6], N'Kaya Guy D. Moukandi [5]

[1] Univ Bretagne Occidentale, CNRS, IUEM, Lab Geosci Ocean,Labex Mer,UMR 6538, F-29280 Plouzane, France.
[2] Univ Colorado, Inst Arctic & Alpine Res, CSDMS, Dartmouth Flood Observ, Boulder, CO 80309 USA.
[3] IFREMER, UR Geosci Marines, BP 70, F-29280 Plouzane, France.
[4] OMP, F-31400 Toulouse, France.
[5] Univ Marien Ngouabi, LMEI CUSI ENSP, BP 69, Brazzaville, Rep Congo.

* Corresponding author : Stéphane Molliex, email address : smolliex@gmail.com

Abstract :

The Congo River is the world's second largest river in terms of drainage area and water discharge. Monitored for decades, a large dataset is available, onshore for both the hydrology and sediment load, and offshore by many paleo-environmental proxies compiled at the Late-Quaternary time-scale. These numerous data allow for accurate calibration of numerical modeling. In this study, we aim to numerically quantify the evolution of sediment supply leaving the tropical Congo watershed during the last 155 ka and to decipher the forcing parameters that control this sediment supply over glacial/interglacial stages. For this, a modified version of the model HydroTrend, that besides morphologic, climatic, hydrologic, lithologic, land cover and anthropogenic factors now also considers sediment deposition on the floodplain, is used. In addition, a method to quantify the impact of natural vegetation changes is developed.

Simulations match well the present-day observed data. They indicate that a significant portion of suspended sediments is trapped on the floodplain. Long-term simulations indicate that environmental changes between glacial and interglacial stages account for a 30% maximum variation of sediment supply. Climatic changes - precipitation and temperature, account for a maximum decrease in sediment supply of 20% during cold periods while conversely, induced land cover changes (loss of forest during colder and dryer stages) lead to enhanced sediment supply up to 30%. Over a longer period, the average sediment supply remained almost constant during glacial and interglacial periods, while peaks may have occurred during a warming period, just before forests had time to recover the catchment, i.e. during post-glacial periods. These moderate changes in sediment export, despite major changes in climate and vegetation cover, can be explained by the efficiency of sediment trapping of large tropical catchments that buffer fluvial fluxes towards the ocean.

Keywords : Glacial/interglacial, Sediment supply modeling, HydroTrend, Vegetation dynamics, Equatorial Africa, Congo watershed, Weathering, Hydrology

1- *Introduction*

Understanding factors and processes controlling sediment yield is crucial for a comprehensive baseline in global denudation rates, fluvial sedimentary archives, biochemical cycles and human impact on sediment fluxes (e.g. Meybeck, 2003; Walling, 2006; Syvitski and Milliman, 2007). Sediment yield can be expressed as a function of various factors including catchment morphology (area, relief, slope), lithology, climatic conditions, tectonics, vegetation, land use, impact of reservoirs (e.g. de Vente and Poesen, 2005; Syvitski and Milliman, 2007; Pelletier, 2012; Vanmaercke et al., 2014). However, the quantification of evolution of sediment yields over time remains a challenge because of the number of processes, the complexity, and the feedbacks of processes involved both on soil denudation and fluvial sediment transport (Picouet et al., 2001). In addition, the relative importance of forcing parameters depends on the size of the catchment and the climatic and tectonic context of its setting and is often poorly understood.

Large tropical catchments contain some of the richest ecosystems on Earth and provide a large part of nutrients to the oceans. Tropical zones have the largest land mass on Earth, a high transport capacity, high erosion rates due to biogeochemical weathering, and thus sediment loads are enhanced by the humid and warm climate (e.g. Xu, 2003; Zhu et al., 2007; Syvitski et al., 2017). Therefore large tropical catchments are playing an essential role in both terrestrial and marine ecosystems. Nevertheless, processes controlling sediment fluxes to the ocean are poorly understood and because of basin size, accurate quantification of these processes over time is often challenging to perform.

The Congo River is the world's second largest river in terms of both drainage area ($3.7.10^6$ km^2) and water discharge (41,000 m^3 s^{-1}) (Laraque et al., 2013). Its catchment can be considered as the most pristine major tropical watershed because it has for example far fewer dams in comparison with other large tropical watersheds such as the Amazon (Latrubesse et al., 2017) or Mekong Rivers (Ellis et al., 2012; Winemiller et al., 2016). However, because it is challenging to acquire *in-situ* data, the Congo basin has experienced much less scientific attention in basin hydrology and sediment supply than other large tropical catchments (Alsdorf et al., 2016). Unlike other major rivers, the contemporary Congo River has always maintained a connection with its deep-sea canyon, allowing for efficient transfer of

Total Suspended Sediment (TSS) directly to the abyssal plain (Rabouille et al., 2009; Vangriesheim et al., 2009). Moreover, Gingele et al. (1998) showed by studying smectite cristallinity that at least 95% of sediment deposited in the deep-sea fan is directly provided by the Congo River, with aeolian contribution being limited. These characteristics make a direct comparison between sediment supply exported from the catchment and the sediment volume deposited in the deep-sea fan possible.

Better understanding of the main controlling factors of sediment yields in Africa is also of interest from a societal perspective. Recent population growth and climatic changes in Africa have important impacts on land cover changes and water resources (e.g. Barnes, 1990; Bruijnzeel, 2004; Zhang et al., 2006; Reichenstein et al., 2013). Reliable information on the variability over time in sediment yield and its sensitivity to land cover or climate changes is therefore crucial for sustainable catchment management (Vanmaercke et al., 2014).

Recently, development of remote sensing tools have allowed for better understanding of the Congo's terrestrial water dynamics (Jung et al., 2010; Beighley et al., 2011; O'Loughlin et al., 2013; Lee et al., 2011; 2014; 2015). Moreover, numerical models such as HydroTrend, based on empirical equations can simulate water and sediment discharge of watersheds and have proven to be able to successfully reproduce basin hydrology over geological times with high accuracy (e.g. Syvitski and Miliman, 2007). These are thus reliable tools for quantifying the role of environmental forcing on fluvial processes, in particular since only 10 % of rivers have observational time series of sediment delivery to the ocean (Syvitski et al., 2005). Of those, few records reach more than a century, which is too short to fully comprehend and unravel processes influencing the fluvial sediment fluxes (Wilby et al., 1997).

However, modeling the Congo's catchment sediment supply towards the ocean is challenging because (i) the size of the catchment, which includes several climatic zones; (ii) the strong variability of land cover over time due to its sensitivity to climate changes, and (iii) of net depositional areas in the catchment that are not always clearly identifiable.

In this study, we simulate the water and suspended sediment discharge exported from the Congo's River basin over the last 155 ka by applying the hydrological transport model HydroTrend, of which the sediment module encompasses the empirical BQART function (Syvitski et al., 1998; Kettner and Syvitski, 2008). This quantification is based on a calibration by *in-situ* present-day data. The variability of water and sediment discharge over the last 155 ka is then modeled from this calibration by using available environmental proxies. These simulations aim to improve our understanding of the factors controlling sediment yield of the Congo catchment and help address societal challenges. In detail, we aim to better understand how the suspended sediment supply varies over one full climatic glacial/interglacial cycle with a focus on transitions. Which are the parameters controlling these variations and how do they control suspended sediment fluxes? We also validate our long-term

sediment flux simulations with published denudation and weathering rates, volumes of sediment deposited offshore and basic weathering proxies determined from marine cores.

2- Environmental setting

The 4,700 km long Congo River drains 3.7 millions of km² of the center of equatorial Africa (Fig. 1), and lies on both sides of the equator. Its heart is constituted by a vast (about 50% of the total drainage area), low gradient (at some locations the slope is less than a few centimeter per kilometer) and shallow perched basin (with altitudes ranging from 300 to 500 m) called "Cuvette Centrale" (Fig. 1A, 1B and 1C). This depression, is the surface expression of a Cenozoic basin, and is surrounded by moderately elevated hills (1000 to 1500 m of elevation) to the North and South, and by a mountain range to the East (the western shoulder of the East African Rift), where elevations reach up to 4100 m (Fig. 1B). These reliefs mainly consist of crystalline basement (e.g. Lee et al., 2015). Terrains with elevations higher than 2000 m only represent 0.4% of the drainage area. Drainage area located in the southern hemisphere represents about 60% of the total drainage area, with a mean elevation of about 200 m higher than the elevation of the drainage area located in the northern hemisphere (Fig. 1A and 1B). The main tributaries of the Congo River are the Oubangui, the Sangha, the group of Batékés Rivers on its right bank, and the Kasaï River on its left bank (Fig. 1). The headwaters of the Congo catchment contain the world's second largest lake by volume and depth (Lake Tanganyika), which holds approximately 17% of the world's fresh water volume (Coulter, 1991) and traps the majority of sediments provided by the upstream part of the catchment (Sichingabula, 1999). In the Cuvette Centrale, two very shallow (3 to 8 m deep) lakes (Tumba and Mai Ndombé) extend for more than 3000 km² and are situated on the left bank of the Congo River (Laraque et al., 1998). These lakes, as well as the "Cuvette Centrale", which is almost permanently flooded, trap a large part of the suspended sediment load. The Congo River delivers water and sediment to the Atlantic Ocean and is directly and permanently connected to an active deep-sea fan through the 1,135 km-long deeply incised submarine Congo Canyon and channels (Babonneau et al., 2002). This hydrographic network remained relatively stable throughout the Quaternary despite sea-level and climatic changes (Guillocheau et al., 2015; Flügel et al., 2015).

Currently, the Congo Basin experiences a humid tropical climate with three main climatic zones: a) equatorial humid in the center of the basin on both sides of the Equator, b) tropical humid with a monsoon season at higher latitudes, and c) tropical semi-arid with a dry season on the northern and southern catchment boundaries (Kottek et al., 2006). The mean annual precipitation is 1,630 mm with a mean temperature of about 24°C at Brazzaville (Bultot, 1972; Alsdorf et al., 2016) (Fig. 2A; Fig. 2B). Vast areas of the central Congo Basin do not experience a dry season, whereas the highlands experience two wet and dry seasons (Boyer et al., 2006). The Congo River crosses the Equator twice and, as a result, experiences always a rainy season somewhere in its basin during the year (Fig. 2A and

2D). The wet season for the southerly flowing tributaries is from April to September (e.g. the Oubangui River) and for the northerly flowing tributaries from October to May (e.g. the Kasai River). This results in a typically equatorial hydrological regime (Rodier, 1964; Martins and Probst, 1991) with limited monthly discharge fluctuations (Fig. 2E; 3A). As an example, for the Congo only two minor peak events in December and May and two minor low flow events in August and March occur (Coynel et al., 2005; Laraque et al., 2009; 2013a) (Fig. 3A). Intrinsically, the Congo River experiences probably the most regular and uniform hydrologic regime on Earth since its mean monthly discharge ratio (maxQ/minQ) is close to 2 and the extreme monthly discharges, recorded from 1902 onwards, range only from 23,000 to 75,500 $m^3 s^{-1}$ (Alsdorf et al., 2016). The inter-annual ratio is only 1.65 with annual discharges ranging from 33,300 to 55,200 $m^3 s^{-1}$ (Alsdorf et al., 2016). The height of the water table, inferred from lake levels (Crétaux et al., 2011; Becker et al., 2014) varies by 80 mm during the year and follows the same trend as the water balance (Precipitation minus Evapotranspiration) (Fig. 2E). Water specific discharge (runoff) stays however almost constant (35 ± 5 mm), highlighting a good relationship between surface and underground water that allows for buffering the monthly river discharge and explains part of the low variability of the hydrologic system.

The "Cuvette Centrale" is mainly covered by evergreen and swamp forest and surrounded by savannah vegetation (De Namur, 1990) (Fig. 2C and Fig. 2F). During the wet season, most of these forests are flooded, while during the dry season, they partially or completely dry (Laraque et al., 1998; Coynel et al., 2005). Anthropogenic disturbances such as sewage inputs, intensive agriculture, deforestation, and dams have not yet had a significant impact on the Congo River, which has therefore not developed any of the global change syndromes observed for most of the world's largest basins (Meybeck, 2003; Coynel et al., 2005). And therefore, the sediment dynamics are still mostly in a natural state.

The Congo River currently transports a total of 87 Mt yr^{-1} of matter to the ocean (Laraque et al. 2009, 2013b). Only one third is constituted by suspended sediment load (SSL) while the main part of matter exported is dissolved (Laraque et al. 2009, 2013b) (Fig. 3B). No accurate data is available for bed load. As for the water discharge, the mean monthly suspended sediment load is also uniform. The total dissolved matter is well correlated to the water discharge, conversely to the SSL (Fig. 3C; 3D). Because of the scarcity of high slope areas in the catchment (less than 0.0005 % of the drainage area has slopes higher than 45°), potential landslides triggered by earthquakes in upstream Congo are unlikely to significantly impact the total suspended sediment load of the catchment.

3- Data and Method

Our simulations were performed by removing part of the Congo Basin located upstream of Lake Tanganyika. The area upstream of Lake Tanganyika, that mainly drains the East-African Rift System, does not significantly contribute to the sediment flux towards the ocean as this lake traps large

portions of the upstream sediment supply (Sichingabula, 1999). For this study, the Congo River outlet was considered at Brazzaville, about 480 km upstream the Congo's actual river mouth (Fig. 1A, 1C). This in order to (i) calibrate our simulations with *in-situ* data available at the Brazzaville's gauging station; and (ii) avoid the potential effect of sea-level fluctuations over glacial-interglacial stages to the catchment, since the erosive regression of the Congo channel due to sea-level regressions does not affect the catchment upstream Brazzaville, as shown by the location of the major knickpoint in the longitudinal profile of the river just downstream Brazzaville (Fig. 1C). Our strategy was to calibrate our simulations using present-day data, before simulating over two different timescales, the last 23 ka and the last 155 ka, by integrating environmental changes, inferred from both marine and continental proxies available for the study area. Simulations over these two different timescales aimed to test the sensibility of the model resolution and also to study the the impact of different controlling factors during climate transitions periods. Furthermore, we included to the classic HydroTrend model the possibility to consider trapping in the alluvial plain, when the discharge exceeds bankfull. We also developed a new methodology to consider vegetation cover variations that can occur between glacial and interglacial periods.

3.1 General principles of HydroTrend

The HydroTrend model allows for daily simulation of discharge and sediment load leaving a river system with high accuracy over long periods of time (Syvitski et al., 1998). The model incorporates basin properties and biophysical processes to compute the hydrological balance (Kettner and Syvitski, 2008). For long-term simulations, HydroTrend has proven to be able to reproduce reliable fluvial sediment yield if appropriate assumptions about past climate and land use are made (Syvitski and Morehead, 1999; Kettner and Syvitsky, 2009). The structure and modules of HydroTrend have been described in detail by Syvitski et al. (1998) and Kettner and Syvitski (2008), and will not be iterated here. However, key equations to compute water discharge, sediment load, and trapping efficiency will be described below.

Based on the classic water balance equation, fluvial water discharge (Q) is determined by basin area A (km^2), precipitation P ($m\ yr^{-1}$), evapotranspiration Ev ($m^3\ s^{-1}$) and water storage as groundwater and its release Sr ($m^3\ s^{-1}$) (Eq. 1).

$$Q = A\sum_{i=1}^{ne}(P_i - Ev_i \pm Sr_i) \quad \text{(Eq. 1)}$$

Here *ne* is the number of simulated epochs (time periods with more or less similar or linear changing environmental conditions), each including multiple years, and *i* is the daily time step. Following Eq. (1), five hydrological processes are taken into consideration: rain (Q_r), snowmelt (Q_n), glacial melt (Q_{ice}), evaporation (Q_{Ev}) and groundwater discharge (Q_g) (all in $m^3\ s^{-1}$) (Eq. 2):

$$Q = Q_r + Q_n + Q_{ice} - Q_{Ev} \pm Q_g \quad \text{(Eq. 2)}$$

The long-term suspended sediment load $\bar{Q}s$ (kg s^{-1}) is computed by applying the semi-empirical BQART equation described by Syvitski and Milliman (2007) (Eq. 3):

$$\bar{Q}_s = \omega B \bar{Q}^{0.31} A^{0.5} \bar{R} T \quad \text{(Eq. 3)}$$

The B term (non-dimensional) being estimated as:

$$B = IL(1 - T_e)E_h \quad \text{(Eq. 4)}$$

where ω is the proportionality coefficient defined to be 0.02 kg s^{-1} km^{-2} °C^{-1} (Syvitski and Milliman, 2007), $\bar{Q}$ and $\bar{R}$ are respectively non-dimensional water discharge at the river mouth and maximum basin relief, following the procedure as $\bar{Q} = \left(\frac{Q}{Q_0}\right)$ and $\bar{R} = \left(\frac{R}{R_0}\right)$, where Q_0 is equal to 1 m^3 s^{-1}, and R_0 equals 1 m. T is the temperature at the basin outlet (°C). I, L, T_e, and E_h are non-dimensional parameters, where I is a glacial erosion factor to represent the impact of glacial erosion processes, L is the basin-averaged lithology factor to express the hardness of rock, and Te is the trapping efficiency by natural and/or human reservoirs. Eh is the soil erosion factor related to human activities (Syvitski and Milliman, 2007; Kettner and Syvitski, 2008) which is adapted for our case to consider vegetation changes (see section 3.3.2 for more details).

To generate daily SSL fluxes, a stochastic model (Psi) is applied (Eq. 5; Morehead et al., 2003).

$$\left(\frac{Q_{s_i}}{\bar{Q}_s}\right) = \psi_i \left(\frac{Q_i}{\bar{Q}}\right)^C \quad i = 1 : m \quad \text{(Eq. 5)}$$

where m is the total number of days (i) being modeled per epoch. The Psi model captures the inter- and intra-annual variability of SSL leaving the river mouth following Eqs. (6) to (9) (Morehead et al., 2003; Syvitski et al., 2005):

$$E(\psi) = 1 \quad \text{(Eq. 6)}$$

$$\sigma(\psi) = 0.763(0.99995)^{\bar{Q}} \quad \text{(Eq. 7)}$$

$$E(C) = 1.4 - 0.025T + 0.00013R + 0.145 \ln(\bar{Q}_s) \quad \text{(Eq. 8)}$$

$$\sigma(C) = 0.17 + 0.00000183\bar{Q} \quad \text{(Eq. 9)}$$

E and σ denote respectively the mean and standard deviation of a random variable Ψ. The random variable changes on a daily time step and has a log-normal distribution. C is a normal distributed rating coefficient that varies over a time step of one year (Syvitsky et al., 2000). For these two variables, the standard deviation depends on the mean discharge, with a power relation for ψ. These equations imply that small rivers have a larger variance in C, while larger rivers have a smaller variance. Notice that for short-term simulations (years to decades), because of the nature of incorporated variability (Eq. 5 to 9), the daily mean suspended sediment load Q_{Si} might not exactly match the long-term mean suspended sediment load $\bar{Q}_s$ as computed by BQART (Eq. 3). However, these two parameters converge in long-term simulations (hundreds to thousands of years).

Because of the basin size and insignificant annual variability in discharge and sediment load of the Congo watershed, $\sigma(C)$ (Eq. 9), using Morehead et al. (2003) provided a significant higher annual variability compared to field observations. We recalculate the $E(C)$ parameter specifically for the

Congo based on 16 years of regularly monitoring of annual sediment load data (PEGI program, Laraque et Orange, 1996; HYBAM, 2016). The observed annual standard deviation is 12 % while Eq. 9 predicts about 40 %. We thus recalibrated Eq. 9 to better reflect variations in sediment for the Congo River (Eq. 10):

$$\sigma(C) = 0.17 + 0.00000056\bar{Q} \quad \text{(Eq. 10)}$$

The trapping efficiency *Te* by natural reservoirs larger than 0.5 km^3, such as lakes, is calculated by HydroTrend using the equation of Brune (1953) following Vörösmarty et al. (1997) when multiple reservoirs are represented in a catchment:

$$T_e = \sum_{j=1}^{m}\left(1 - \frac{0.05}{\sqrt{\Delta\tau_j}}\right) \quad \text{(Eq. 11)}$$

Here $\Delta\tau_j$ is the approximated residence time per sub-basin *j* and is estimated by

$$\Delta\tau_j = \frac{\sum_1^{n_i} V_i}{Q_j} \quad \text{(Eq. 12)}$$

where V_i is the operational volume of the reservoir *i*, and Q_j is the discharge at the mouth of each sub-basin *j*. Specifically to this study, we included in the model the possibility of additional trapping by floodplains and wetlands. Many large catchments contain alluvial plains. When bankfull discharges are exceed, sediment can be trapped within an alluvial plain. For the model, we considered that as the discharge exceeds the bankfull threshold at a certain location (based on upstream area or certain elevation in the drainage basin), sediment load is trapped on the floodplain (Qsi_{bk}) which is estimated as:

$$Qs_{ibk} = (Q_i - Q_{bk}) \times C_{si} \quad \text{(Eq. 13)}$$

where the accessible water is daily calculated as total discharge (Q_i) minus the bankfull threshold (Q_{bk}), and C_{si} is the daily sediment concentration. When the bankfull threshold is reached, we assume that 100% of suspended sediments is deposited in the floodplain.

3.2 Input parameters for short-term calibration.

The morphological characteristics of the catchment, including river length, drainage area, the delta slope, hypsometry, latitude, location of reservoirs, are extracted from the Shuttle Radar Topography Mission Digital Elevation Model (SRTM DEM) with a spatial resolution of 30 arc-sec (Farr et al., 2007). For hydrological properties, the average velocity of the Congo River at its main Maluku Trechot gauging station (30 km upstream Brazzaville, Fig. 1) is 1.23 m s^{-1} (Laraque et al., 1995). Groundwater storage (350 ± 250 km^3), groundwater coefficient (15,000 m^3 s^{-1}) and groundwater exponent (1.4) are deduced from satellite-inferred lakes level fluctuations (HydroWeb database: http://www.legos.obs-mip.fr/en/soa/hydrologie/hydroweb/; Crétaux et al., 2011; Becker et al., 2014). The mean saturated hydraulic conductivity, related to soil texture is chosen to be 315 mm/day, corresponding to a moderate coarse sandy loam (Bear, 1972). A lithology factor of 0.5 (*L*) is assigned

using the classification scheme of Syvitski and Milliman (2007). All input parameters used are summarized in Table 1.

Mean monthly temperatures at Brazzaville are compiled from the Worldclim database (Hijmans et al., 2005). Mean monthly precipitations are compiled both from the Tropical Rainfall Monitoring Mission (TRMM) (Wang et al., 2014) and from 277 *in-situ* climate stations compiled in the SIEREM database (Boyer et al., 2006) (locations are provided in Fig. 2A). This compilation highlights a good correlation between monthly precipitation and their standard deviation at the basin scale (R^2 = 0.9), which suggests a low inter-annual variability and allows for the determination of the temporal standard deviation of precipitation applied to TRMM data. For the Congo basin, present-day Equilibrium-Line Altitude (ELA) of glaciers is about 4500 m (Osmaston and Harrison, 2005). Glacial erosion is thus currently negligible since only an insignificant part of the Congo catchment lies above this elevation.

3.3 Input parameter for long-term simulations

Since the hydrographic network remained almost unchanged (Flügel et al., 2015) and tectonics are stable throughout the Quaternary (Guillocheau et al., 2015), we can assume that only climate and land cover significantly influence water and sediment discharge during the last 155 ka. Given the high temporal resolution of the input data, the resolution of our simulations can be constrained to 200 years for the 0-23 ka period and 1,000 years for the 0-155 ka simulation.

3-3-1- Climate changes

Past precipitation and temperature can be reconstructed using proxies from local marine cores and global climatic models (Fig. 4). For precipitation, we use the $\delta^{18}O$ curve compiled from core MD03-2707 (Weldeab et al., 2007) located in the Gulf of Guinea about 1000 km NW of the Congo's outlet. This proxy is representative of the intensity of the West African Monsoon (Weldeab et al., 2007, Caley et al., 2011). For temperature, we use interpolations of Weijers et al. (2007), who directly interpolated the mean atmospheric temperature (MAT) from the Methylation index of Branched Tetraethers (MBT) and the Cyclisation ratio of Branched Tetraethers (CBT) in core GeoB6518-1 for the last 25 ka, located close to the Congo River outlet (Fig. 1). In addition to these data, for ages older than 25 ka, we used the Sea Surface Temperature curve (SST) provided by Weldeab et al. (2007) from core MD03-2707, since a correlation can be made at these latitudes between sub-surface marine and aerial temperatures (Weaver et al., 2001). These data were then calibrated in terms of annual rainfall and temperature by using present-day and Last Glacial Maximum (LGM) global climatic models (CCSM4; Gent et al., 2011) (Fig. 4). Monthly variations are calibrated with simulations of Kutzbach et al., (1998) and Jolly et al., (1998). A first order variation of ELA is interpolated from local estimations at LGM of Osmaston and Harrison (2005), following the intensity of Marine Isotopic Stages (Lisiecki and Raymo, 2005). Note that less than 1 % of the catchment is concerned by glacial erosion during the

coldest phases (Osmaston and Harrison, 2005). Therefore, glacial erosion has only a limited impact during the cold stages on the fluvial sediment flux.

3-3-2- Land cover changes

Long-term land cover changes are constrained using recent data as well as a detailed pollen study of core KZaï-02 (Dalibard et al., 2014), collected in 1998 on the Congo deep-sea fan, 248 km off the Congo River mouth, during the ZaïAngo1 cruise (Savoye et al., 1998) (Fig. 1) to identify historical land cover changes. In order to quantify the impact of these changes in our simulations, we used an approach based both on a satellite derived land cover map (GLC-SHARE; Latham et al., 2014) and on monthly NDVI maps MOD13A3 provided by NASA (https://lpdaac.usgs.gov/dataset_discovery/modis/modis_products_table/mod13a3; Huete et al., 2002) (Fig. 5). NDVI (Normalized Difference Vegetation Index) (Tucker, 1979) is a widely used index in remote sensing studies (e.g. Xie et al., 2008). It is based on green vegetation and varies between 0 for bare soil to 1 if the soil is entirely covered, so protected by vegetation (e.g. Crippen, 1990). We compiled a mean annual NDVI map for the Congo catchment by averaging 12 contiguous monthly NDVI maps MOD13A3 (period 2000-2001). Annual NDVI ranges from 0.35 for the sparsest grasslands and crops to 0.85 for the densest rainforests (Fig. 5C). We then computed the relationship between mean annual value of NDVI ($NDVI_y$) and the proportion of forested areas for 100 x 100 km tiles in the catchment *Fs* (Fig. 5D). A correlation of $R^2 = 0.52$ was found between forests and the $NDVI_y$. This relationship is stronger if only forests located below 900 m of elevation are involved ($R^2 = 0.68$) (Fig. 5D), the correlation equation being:

$$NDVI_Y = 0.00187 \times Fs + 0.574 \quad \text{(Eq. 14)}$$

Within the catchment, the elevation of 900 m corresponds to the lowest limit of mountainous type forests. We also compiled an evolution curve of the percentage of non-mountainous forests in the catchment using pollen data (Dalibard et al., 2014) and determined equivalent paleo-NDVI values from each epoch (age step) by using the correlation equation (Eq. 14) (Fig. 4E; 4F).

We can then determine a soil cover factor *Cf* from these paleo-NDVI values. *Cf* = 0 if vegetation cover is negligible (i.e. bare soil), and *Cf* = 1 if the vegetation entirely covers the soil. A maximum soil cover factor *Cf* can be determined by using the maximum amplitude of present-day *NDVIy* values (i.e. 0.85 for densest rainforest and 0.35 for sparsest grasslands and crops) and assuming that $Cf_{max} = 1$ for the highest NDVI value (0.85; 100 % of forests) and $Cf_{max} = 0$ for the lowest NDVI value (0.35; 0% of forests) (Fig. 4F). The minimum soil cover factor can be calculated from the amplitude of NDVI determined from the correlation between present-day NDVI and proportion of forest (eq. 14), assuming that $Cf_{min} = 1$ for 100 % of forests (NDVI = 0.76) and $Cf_{min} = 0$ for 0 % of forest (NDVI = 0.57). These values can be assumed as minimum because where there is no forest nowadays,

vegetation is mainly constituted by savannah. But during colder periods, such as during the LGM, non-forested vegetation was probably much sparser, with a lower NDVI value.

In that case, C_{max} and C_{min} are thus calculated as following:

$$Cf_{max} = (0.85 - 0.35)F + 0.35 \quad \text{(Eq. 15a)}$$

$$Cf_{min} = (0.76 - 0.57)F + 0.57 \quad \text{(Eq. 15b)}$$

This parameter is integrated in the BQART equation by using the erosion factor parameter *Eh* (Eq. 4), such that:

$$E_h = (1 - Cf) \times 2 \quad \text{(Eq. 16)}$$

We add a factor of 2 to ensure that a normal erosion factor (Eh =1) corresponds to a moderate vegetation cover, which has a $NDVI_y$ of 0.5.

Ratios of erosion factors between grassland, savannah and non-mountainous forests are consistent with ratios obtained from *in-sit*u measurements of soil erosion in Africa under similar environmental conditions (Dunne, 1979; Lal, 1985; El-Hassanin et al., 1993).

4- Results

4.1 Model calibration with present-day in-situ data

We first calibrated simulated water discharge to 114 years of monthly observed data available for Brazzaville/Kinshasa gauging station (1902-2016) (GRDC, 2016; HYBAM, 2016) (Fig. 6). A good correlation between the ranked monthly discharges observed and simulated by HydroTrend can be noticed (Fig. 6B), proving that HydroTrend is able to accurately simulate the Congo discharge at an annual scale, despite the large basin size and the heterogeneous climate of the catchment. The annual-averaged simulated discharge is 41,650 $m^3 s^{-1}$ and compares well with observations (41,480 $m^3 s^{-1}$). At a monthly scale, simulated discharges match observed data for May to October, while the model underestimates by about 20% the discharges from November to January and overestimates discharges by about 20 % from February to April (Fig. 6C). These uncertainties may be due to difference of drainage area and/or morphology between the northern hemisphere (~ 40 % of the total drainage area, 600 m of mean elevation) and the southern hemisphere (~ 60 % of the total drainage area, 800 m of mean elevation) parts of the catchment.

To calibrate SSL (Suspended Sediment Load), we used in-situ monitoring data at Brazzaville station, collected through several sources: preliminary survey in the 70s (Giresse and Moguedet, published in Kinga-Mouzeo, 1986), continuous once-a-month survey between 1987 and 1993 (PEGI program, Laraque et Orange, 1996) and continuous once-a-month survey from 2005 to present-day (HYBAM,

2016). Some complementary data are also available from Spencer et al., (2016). To compare observed and simulated data we simulated 20 years of daily sediment discharge. First, a simulation of SSL without any trapping shows a large discordance between observed and simulated data (Fig. 7A). Then, we added a classic trapping, that would most likely occurs in the low-slope lands of the Cuvette Centrale, which could be interpreted similarly as trapping in a lake. Simulation shows that this kind of trapping is not sufficient to match *in-situ* data, especially during high-discharge events (Fig. 7B). To adjust for these high-discharge events, we considered an additional trapping, within the wetlands of the floodplain. This kind of trapping concerns only sediments exported above bankfull discharges, that correspond to the discharge needed to flood the alluvial plain. Calibrating to the simulations, we get the best results when bankfull discharge is 33,000 m^3 s^{-1}. This is about 20% lower than bankfull discharge calculated from empirical equations (Andreadis et al., 2013), and particularly low in comparison with mean annual discharge because some parts of the alluvial plains are almost permanently flooded. After taking this wetland trapping into account, simulated sediment load data match the observed data well (Fig. 7C). The mean SSL is respectively of 1072 kg s^{-1} for simulated data and 974 kg s^{-1} for in-situ data. This difference can be explained by the lack of *in-situ* measurements during very high-discharge events (> 65,000 m^3 s^{-1}) that can lead to an underestimation of SSL. This underestimation is common as reliable sediment concentration measurements during high-discharge events are almost impossible to measure (e.g. Syvitski et al., 2003).

4.2 Simulations of the last 155 ka.

Fig. 8A and B show the 500-year running averages of mean annual simulated sediment and water discharge leaving the Congo catchment over the last 155 ka. A change in water discharge correlated with climatic periods can be observed, with a mean discharge ranging from 40,000 to 50,000 m^3 s^{-1} during warm stages (MIS 1, 5a, 5c, 5e) and around 35,000 m^3 s^{-1} during main cold stages (MIS 2, 4, 6) (Fig. 8). Changes in water discharge are often drastic during transitional periods. Sediment discharge (Fig. 8) fluctuates more frequently. The minimum and maximum values (in grey Fig. 8) are calculated with respect to assumptions about the vegetation index (see part 3.3.2). The mean SSL curve (in black Fig. 8) overall indicates a negative correlation between water discharge and suspended sediment load. Differences between lower (in warm periods) and higher (in cold periods) sediment discharges can reach up to 50%, from 950 to 1500 kg s^{-1}. A focus on water and sediment discharges leaving the Congo catchment since the last 23 ka with a higher resolution is presented in Fig. 9. It aims to improve constrains on inter-annual variability and better understand the transitions between warm and cold periods. As already shown for the 155 ka simulation, mean annual water discharge (in black Fig. 9A) is about 25% less during the LGM. The inter-annual variation (in gray Fig. 9A) is also less during the LGM (15% compared to 30% today). Mean annual SSL varies between 700 and 1900 kg s^{-1} over the last 23 ka period (Fig. 9C), but the mean SSL averaged on a running mean over 100 years shows variations between 950 to 1300 kg s^{-1}, with an overall average of about 1100 kg s^{-1} (in black Fig. 9D).

The inter-annual discharge variability is not significantly different between LGM and present-day and the mean annual SSL is only about 10% higher during the LGM (in gray Fig. 9D). The highest SSL corresponds to a post-glacial period (16-12 ka) and a short event around 5-6 ka (further discussed in section 5.1). Two simulations, respectively without and with vegetation changes were performed (Fig. 9B and 9C). They aimed to highlight the importance of vegetation changes, which largely guide second order variations and are responsible for the two high sediment periods previously mentioned. A 20 year daily simulation that considers LGM environmental conditions (21 ka) was also performed in order to compare SSL between glacial and interglacial (present-day) periods (Fig. 10A). During LGM, the water discharge is lower, but because of the less dense vegetation cover, the concentration of sediment is higher. It results in a slightly higher SSL during LGM, and showing an increase of about 15% (1221 kg s^{-1} at LGM versus 1072 kg s^{-1} today). These results suggest that during cold periods, the climatic conditions are theoretically less favorable to the production of sediment, notably because of the lower precipitation rate. But at the same time, the regression of rainforests enhanced soil erosion and thus sediment production. Therefore, the two effects have opposite consequences on sediment production. Graphs of Fig. 10B and Fig. 10C aim to decipher the relative contribution of climate conditions (temperature and precipitation) (red curve) and vegetation cover (green curve) with respect to mean sediment load (black curve). Data are normalized for comparison with present-day. Except during warm periods (MIS 1, 5c and 5e), climate factors typically cause a decrease in sediment production in comparison to present-day. Decreases of forested land during colder periods enhanced sediment production. This explains why the sediment load varies only by 10-15% during most of the last 155 ka (except for some relatively short periods), while variations in climate conditions and vegetation cover could impact up to 30% the sediment load between the more and the less favorable periods (Fig. 10C). It also implies that peaks in sediment supply most likely occur when climate begins to warm, after a cooling period but vegetation had no chance yet to fully recover and reconquer the catchment, i.e. during post-glacial periods. In the case of the last deglaciation (16-12 ka) this peak reached about 1300 kg s^{-1}, i.e. 20 % higher than what is currently observed.

By extrapolating the period to 155 ka, highest simulated SSL peaks occurred during the MIS 5, with about 30 % more sediment than currently observed, and when climate changes were very rapid and intensive, between the cold (MIS 5b and 5d) and the warm (MIS 5a, 5c, 5e) inter-stages.

5- Discussion

5.1 *Importance of vegetation cover changes*

Simulation results suggest there is a stronger control of vegetation cover on sediment load for the Congo catchment over precipitation and temperatures. Vegetation cover partly protects soil from

eroding by intercepting raindrops, enhancing infiltration, transpiring soil water, and increasing surface roughness (Rogers and Schumm, 1991; Castillo et al., 1997; Gyssels et al., 2005; Roller et al., 2012, El Kateb et al., 2013). In tropical zones the vegetation cover is strongly controlled by climatic conditions (Elenga et al., 2004; Dalibard et al., 2014). The sea surface temperature controls upwelling and monsoon intensity (Maley et al., 1997) and directly impacts tropical rainforest development. During the LGM, tropical rainforests decreased by about 70-80 % for the Congo catchment (Jolly et al., 1998; Rommerkirchen et al., 2006). Simulations suggest that this decrease in rainforest could be responsible for enhancing sediment production by more than 30 %, while external climatic variations account only for a 20 % decrease in sediment during glacial stages. A peak of sediment load occurred at around 5 ka (Fig. 9D). This sediment peak reflects a decrease in rainforest coverage during a period when no change in climatic condition is detected (Fig. 10B) (Bayon et al., 2012; Dalibard et al., 2014). This event, probably more accurately dated by pollen studies onshore at 3 ka (e.g. Elenga et al., 2004) instead of the 5 ka that was dated by offshore proxies, was associated to a global intensification of erosional processes (Maley, 1992; Bayon et al., 2012). It was interpreted as resulting from a potential change in rainfall variability, due to the setting of convective atmospheric systems leading to an alternation between dry periods and very strong precipitation events responsible for an increase of runoff and a decrease of water infiltration (Maley, 1982; Maley et al., 2000). The presence of human activities in the forest at this time, evidenced by archeological studies (Wotzka 2006; Brncic et al. 2007; Morin-Rivat et al., 2014) could also be a forcing factor, limiting forest development, as suggested by Bayon et al. (2012), although the specific role of human impact is still largely questioned (Neumann et al., 2012; Maley et al., 2012).

5.2 *Mass budget comparison between exported sediments, denudation and weathering rates and sediments deposited offshore.*

Present-day specific sediment load exported from the Congo catchment, estimated from the most recent river load compilation (Laraque et al., 2013b) is 2,725 kg s^{-1} (1,046 kg s^{-1} of TSS and 1,679 kg s^{-1} of dissolved matter). This corresponds to an erosion rate of about 23 t km^{-2} yr^{-1}, consistent with the 19 t km^{-2} yr^{-1} indicated by previous studies (NKounkou and Probst, 1987; Summerfield and Hulton, 1994). Present-day global mass budget deduced from geochemical analyses is 13 t km^{-2} yr^{-1} (Gaillardet et al., 1995). Different estimates are therefore of the same order of magnitude. At longer timescales (10^5-10^6 years), our results suggest denudation rates of about 26 t km^2 yr^{-1}, considering a constant ratio between suspended and dissolved sediment load. Denudation rates deduced from cosmogenic studies suggest a similar rate of about 27 t km^2 yr^{-1} for the Congo basin (Al-Gharib, 1992), which is in the same range as other cosmogenic studies for drainage basins in central and western Africa, located in similar climatic, morphologic and lithologic setting. For example, 8 to 22 t km^{-2} yr^{-1} for the Burkina-Faso craton (Brown et al., 1994) and 7 to 16 t km^{-2} yr^{-1} for the Nyong River in Cameroon (Regard et al., 2016). These estimates are stable over long geological timescales (10^7-10^8 years), since mass

budgets determined from morphological studies suggest rates of 14.6 t km^{-2} yr^{-1} (Guillocheau et al., 2016) to 16-22 t km^{-2} yr^{-1} over the last 35 Ma (Leturmy et al., 2003), in the same range as other but similar catchments in central and western Africa (Beauvais and Chardon, 2013). This good agreement between modern and long-term sediment fluxes was also evidenced in similar settings (lowland areas of large catchments), such as the Amazon (Wittmann et al., 2011) but also for landscapes considered in equilibrium (Clapp et al., 2001; Matmon et al., 2003; Vance et al., 2003). Offshore the Congo, most of the sediments are deposited within the deep-sea fan (Droz et al., 2003; Savoye et al., 2009) since the outlet of the watershed is connected to the deep canyon indifferently during high or low eustatic stages (Babonneau et al., 2002). Volumes of sediment deposited in the most recent turbidite fan (axial fan) were accurately estimated for several cycles of sedimentation over the last 210 ka (Picot, 2015; Picot et al., 2016). The periods concerned are 0-11 ka; 11-75 ka; 75-130 ka; 130-210 ka. Decompacted volumes given by Picot (2015) were transformed into mass using a density of 1.8 t m^{-3}, allowing for comparison to simulated riverine sediment loads. These volumes can be compared to budgets deduced from our sediment load results since more than 95 % of sediment preserved in the deep-sea fan is provided by the Congo River (Gingele et al., 1998). The total decompacted volume of sediment of the axial fan is about 8,500 km^3 (Picot et al., 2016) recently re-evaluated to 7,700 km^3 (Laurent et al., 2017), which corresponds to an equivalent erosion rate of 18.8 ± 0.9 t km^{-2} yr^{-1} or a mean sediment load of about 2200 ± 100 kg s^{-1}. These sediment loads are of the same order of magnitude as the previously published erosion rates, determined using different independent methods (Al-Gharib, 1992; Gaillardet et al., 1995; Leturmy et al., 2003; Guillocheau et al., 2016). This indicates that a large part of exported matter, including dissolved matter, is preserved in the sediment of the deep-sea fan. Two thirds of the matter exported from the Congo catchment is dissolved (Laraque et al., 2013b), but the biogenic part of marine sediments represents less than 30 % of the turbidite fan sedimentation. This biogenic part consists mainly of siliceous biogenic sediments (Schneider et al., 1997, Hatin et al., 2017). For the Amazon, biogenic silica is formed as soon as the dissolved load comes in contact with the marine domain, because of the change in redox conditions, but this biogenic silica also very rapidly weathers into authigenic K-Fe-rich aluminosilicates (Michalopoulos and Aller, 2004). K-Fe-rich aluminosilicates are present in the Congo sedimentary system (Giresse et al., 1988; Amouric et al., 1994) suggesting that the same kind of processes may occur for the Congo dissolved matter. The rapid recycling of biogenic silica to authigenic clays might explain why the biogenic part in marine sediments is much lower than dissolved matter exported from the catchment.

In detail, decompacted volumes estimated from Laurent et al. (2017) are: 992 km^3 for the 0-11 ka period, i.e. 43.9 t km^{-2} yr^{-1}; 3,730 km^3 for the 11-75 ka period, i.e. 28.4 t km^{-2} yr^{-1}; 904 km^3 for the 75-130 ka period, i.e. 8 t km^{-2} yr^{-1} and 2,073 km^3 for the 130-210 ka period, i.e. 12.6 t km^{-2} yr^{-1}. The period 0-75 ka presents a corresponding sediment load about three times higher than for the period 75-210 ka, which is not consistent with results of the sediment load simulations. The simulations do not

suggest a significant difference of sediment inputs between these two periods (1,151 kg s^{-1} for 0-75 ka; 1,173 kg s^{-1} for 75-155 ka). A remobilization of older sediments in the most recent deposits might explain this difference but the good stacking and preservation of turbidite features over the last 800 ka (Droz et al., 2003; Marsset et al., 2009) argues against this assumption. Another possible explanation is that very large catchments such as the Congo may buffer high-frequency oscillations (Métivier and Gaudemer, 1999; Castelltort and Van den Driessche, 2003) by the more or less temporary storage of sediments on the alluvial plain (Wittmann et al., 2011). Indeed, large pulses of mobile sediment may be buffered if the amount of sediment stored in a floodplain is large relative to the sediment load. Similar, the stream may maintain an important load of sediment when hinterland sediment production is reduced, due to the presence of transportable debris stored in the floodplain (Phillips, 2003). The agreement of modern and long-term output fluxes of the Congo could thus be explained by this buffering capacity of the floodplain and/or of the estuary (Eisma and Kalf, 1984), while sediment loads deduced from our simulations and those deduced from stratigraphic records may mismatch over shorter wavelength ($< 10^5$ yrs) due to the same buffering effect, as demonstrated by Castelltort and Van den Driessche (2003) and Simpson and Castelltort (2012) for large watersheds. In similar studies, the size of the catchment has also been already evoked as a parameter allowing for the buffering of water and sediment discharges over a glacial/interglacial cycle (Kettner and Syvitski, 2009). Note also that only suspended sediment load is simulated here, dissolved matter and bedload might have a different behavior with respect to trapping and release in the catchment and thus could also contribute to explain a mismatch between sediment exportation and stratigraphic records over short wavelength.

5.3 Simulation comparison with chemical proxies deduced from marine cores

Numerous oceanographic cruises were conducted in the study area during the last decades (Cochonat and Robin, 1992; Cochonat, 1998; Savoye, 1998; Marsset and Droz, 2010; Droz and Marsset, 2011). These cruises allowed for a detailed, comprehensive offshore dataset which led to many environmental studies that aimed to better understand regional paleo-environmental conditions and their implications in term of source-to sink water and sediment budgets and continental weathering over a certain period (e.g. Bayon et al., 2012; Dalibard et al., 2014; Picot et al., 2016; Hardy et al., 2016; Hatin et al., 2017). From these studies, we retain the main classically used proxies in relation to water and sediment transport capacity and intensity of weathering for comparisons with water and sediment supply determined from the here presented model simulations. Note that due to the large size of the catchment and its ability to buffer small wave-length variations in environmental conditions, chemical proxies extracted from marine cores may only approximately represent continental conditions and should be used with caution. Most of the data used were obtained from core KZaï-02 drilled during ZaïAngo1 cruise (Savoye et al., 1998).

548 The chemical erosion of silicates (i.e. weathering) is defined by the alteration of K-feldspar to
549 kaolinite. A high Al/K ratio reflects a high abundance of kaolinite and thus a high weathering degree
550 (e.g. Schneider et al., 1997). We thus used an Al/K semi-quantitative ratio measured with a XRF core
551 scanner for core KZaï-02 (Hatin et al., 2017). For core KZaï-01, located very close to KZaï-02 (Fig.
552 1), it was shown that quantitative measurements of Al/K (Bayon et al., 2012) follow a similar trend as
553 semi-quantitative ratios (Picot, 2015), allowing for the interpretation of semi-quantitative values as
554 representative of weathering intensity. Al/K ratio (Fig. 11C) is lower during cold periods indicating a
555 less efficient chemical weathering consistent with a lower water runoff (Fig. 11B) especially during
556 MIS2, MIS4 and MIS5b. At the same time sediment load increases (Fig. 11A) during cold stages,
557 meaning that physical erosion processes get enhanced in comparison with chemical processes. The
558 kaolinite/smectite ratio also reflects the weathering degree (Gingele et al., 1998). The
559 kaolinite/smectite ratio measured for KZaï-02 (Sionneau et al., 2010) (Fig. 11D) follows a trend
560 similar to Al/K ratio but is less clear, since this ratio responds over a large timescale and is very
561 sensitive to the sediment source (Thiry, 2000). Ti/Ca ratio is a tracer of fluvial intensity since titanium
562 is an immobile element in coarse sediment, while calcium resides in easily dissolvable minerals (e.g.
563 Adegbie et al., 2003; Govin et al., 2012). For the Congo, high values of Ti/Ca (Fig. 11E) only
564 occurred during long humid phases (MIS5e and MIS1) and thus do not systematically correlate with
565 water discharge (Fig. 11B). Short wave-length variations of water discharge are probably buffered by
566 trapping capability in the catchment (see discussion in section 5.1) and explain why the Ti/Ca ratio
567 does not accurately reflect the fluvial variation of the Congo. We also computed total organic carbon
568 (TOC) for core KZaï-02 (Picot, 2015) since it correlates well with climate cycles (Fig. 11F). We
569 observe an increase from 1% to 2-3% of TOC during cold periods. Most of this organic carbon has a
570 continental origin for recent periods (late Holocene) (Baudin et al., 2010), but the increase of TOC
571 during glacial stages is not consistent with the decrease in vegetation cover at that same period.
572 Schneider et al. (1997) deciphered continental and marine organic carbon in the Congo's marine
573 sediments over the last 200 ka and demonstrated that terrestrial organic carbon did not fluctuate
574 significantly in time, while fluctuations in TOC over glacial/interglacial stages are mainly controlled
575 by marine organic carbon. During cold periods, primary productivity might be enhanced by strong
576 trade winds which could reinforce upwelling and change thermoclines (Schneider et al., 1997; Berger
577 et al., 2002). The TOC seems thus controlled by the marine organic carbon rate, that is higher during
578 glacial stages while terrestrial conditions are less favorable for the development of vegetation and
579 exportation of organic carbon from the continent (less runoff and more sediment exported, Fig. 11B
580 and C).

581 ## *6- Conclusions*

We numerically simulated water and sediment supply exported to the ocean by the Congo, the second largest river in the world in terms of discharge and drainage area, over the last 155 ka. This work is a first attempt to use the numerical model HydroTrend on such a long time scale and on such a large catchment. In context of the Congo, climate and land cover changes are the main drivers controlling water and sediment supply to the ocean. For this study, numerous calibrating datasets existed over long time scales, allowing for accurate long-term simulations (>10^5 years). Despite the size of the watershed, HydroTrend was able to accurately simulate water discharge and sediment load exported from the Congo. Climate and land cover changes were calibrated using global climate models, marine proxies and remote sensing data. In particular, we developed an original approach for quantifying the impact of vegetation changes. Results show that water discharge is very sensitive to climate, with a decrease in discharge of about 25% during glacial stages. Sediment load is more sensitive to vegetation changes than climate changes themselves. Variations in sediment load can reach up to more than 30% in comparison with present-day during periods when climate began to warm and vegetation did not have the chance yet to grow and extend again, i.e. during post-glacial stages. Overall, despite a decrease in water discharge, the loss of rainforest enhanced soil erosion and thus sediment load slightly increased during glacial stages. We also highlight that trapping is important in the catchment and occurred in the wetlands and flood plains of the lowlands. This trapping act as a buffer for small wave-length environmental variations, making interpretations in a source-to-sink approach more challenging, from a stratigraphic, sedimentologic and chemical point of view. In future, our approach and the novelties we added to HydroTrend could be applied for other large tropical catchments of e.g. Africa, in order to infer the potential effect of environmental changes on water and sediment discharge.

7- Acknowledgements

This work benefited from a State Grant from the French "Agence Nationale de la Recherche (ANR)" in the Program "Investissements d'Avenir" (ANR-10-LABX-19-01, Labex Mer). USA co-author AK was supported through the NSF continuing Grant 0621695. We are grateful to the two anonymous reviewers for their fruitful comments which contributed to improve the manuscript. We thank M. Picot, G. Bayon and N. Freslon for fruitful discussions. The work also benefited from data acquired during oceanographic cruises (Guiness and ZaïAngo).

References cited

Adegbie, A.T., Schneider, R.R., Röhl, U., Wefer, G., 2003. Glacial millennial-scale fluctuations in central African precipitation recorded in terrigenous sediment supply and freshwater signals offshore Cameroon. Palaeogeogr., Palaeoclimatol., Palaeoecol. 197(3–4), 323–333, doi:10.1016/S0031-0182(03)00474-7

Algharib, I., 1992. Apport des isotopes à vie moyenne de l'Uranium et du Thorium, 210Pb et 10Be dans l'étude de l'érosion chimique et physique de deux grands bassins: Amazone et Congo. PhD thesis, Univ. Nice-Sophia Antipolis.

Alsdorf, D., Beighley, E., Laraque, A., Lee, H., Tshimanga, R., O'Loughlin, F., Mahé, G., Dinga, B., Moukandi G., Spencer, R.G.M., 2016. Opportunities for hydrologic research in the Congo Basin. Reviews of Geophysics 54, doi:10.1002/2016RG000517.

Amouric, M., Parron, M., Casalini, C., Giresse, P., 1995. A (1: 1) 7-Å Fe phase and its transformation in recent sediments: An HRTEM and AEM study. Clays and Clay Min. 43, 446–454.

Andreadis, K.A., Schumann, G. J.-P., Pavelsky, T., 2013. A simple global river bankfull width and depth database. Water Resour. Res. 49, 7164–7168, doi:10.1002/wrcr.20440.

Babonneau, N., Savoye, B., Cremer, M., Klein, B., 2002. Morphology and architecture of the present canyon and channel system of the Zaire deep-sea fan. Mar. Pet. Geol. 19, 445–467. doi:10.1016/S0264-8172(02)00009-0

Barnes, R.F.W., 1990. Deforestation trends in tropical Africa. African Journal of Ecology 28, 161-173.

Baudin, F., Disnar, J.-R., Martinez, P., Dennielou, B., 2010. Distribution of the organic matter in the channel-levees systems of mud-rich deep-sea fan (West Africa). Implication for deep offshore source rocks and global carbon cycle. Marine and Petroleum Geology 27, 995-1010.

Bayon, G., Dennielou, B., Etoubleau, J., Ponzevera, E., Toucanne, S., Bermell, S., 2012a. Intensifying Weathering and Land Use in Iron Age Central Africa. Science 335, 1219–1222. doi:10.1126/science.1215400

Bear, J. 1972. Dynamics of fluids in porous media. Courier corporation, 764 pp.

Beauvais, A., Chardon, D., 2013. Modes, tempo, and spatial variability of Cenezoic cartonic denudation : The West Afracan example. Geochemistry, Geophysics, Geosystems 14, doi:10.1002/ggge.20093

Becker, M., Santos da Silva, J., Calmant, S., Robinet, V., Linguet, L., Seyler, F., 2014. Water Level Fluctuations in the Congo Basin Derived from ENVISAT Satellite Altimetry. Remote Sensing 6, 9340-9358. doi:10.3390/rs6109340

Beighley, R.E., Ray, R.L., He, Y., Lee, H., Schaller, L., Andreadis, K.M., Durand, M., Alsdorf, D.E., Shum, C.K., 2011. Comparing satellite derived precipitation datasets using the Hillslope River Routing (HRR) model in the Congo River Basin. Hydrological Processes 25, 3216–3229. doi:10.1002/hyp.8045.

Berger, W.H., Lange, C.B., Wefer, G., 2002. Upwelling history of the Benguela-Namibia system: a synthesis of Leg 175 results. In Wefer, G., Berger, W.H., Richter, C. (Eds.), Proc. ODP, Sci. Results 175, 1–103.

Boyer, J.-F., Dieulin, C., Rouche, N., Cres, A., Servat, E., Paturel, J.-E., Mahé, G., 2006. SIEREM an environmental information system for water resources. 5th World FRIEND Conference, La Havana - Cuba, November 2006 in Climate Variability and Change – Hydrological Impacts IAHS Publ. 308, 9-25.

Brncic, T.M., Willis, M.K.J., Harris, D.J., Washington, R., 2007. Culture or climate? The relative influences of past processes on the composition of the lowland Congo rainforest. Philosophical Transactions of the Royal Society of London B 362(1478), 229–242.

Brown, E.T., Bourlès, D.L., Colin, F., Sanfo, Z., Raisbeck, G.M., Yiou, Y., 1994. The development of iron crust lateritic system in Burkina Faso, West Africa, examined with in-situ produced cosmogenic nuclides. Earth Planet. Sci. Lett. 124, 19 – 33.

Bruijnzeel, L.A., 2004. Hydrological functions of tropical forests: not seeing the soil for the trees? Agriculture, Ecosystems and Environment 104, 185-228.

Brune, G.M., 1953. Trap efficiency of reservoirs. Trans Am Geophys Union 34, 407–418.

Bultot, F., 1972. Atlas Climatique du Bassin Congolais. Publications de L'Institut National pour L'Etude Agronomique du Congo (I.N.E.A.C.), 3° Partie, Température et Humidité de L'Air, Rosee, Température du Sol.

Caley, T., Malaizé, B., Revel, M., Ducassou, E., Wainer, K., Ibrahim, M., Shoeaib, D., Migeon, S., Marieu, V., 2011. Orbital timing of the Indian, East Asian and African boreal monsoons and the concept of a "global monsoon." Quat. Sci. Rev. 30, 3705–3715. doi:10.1016/j.quascirev.2011.09.015

Castelltort, S., Van Den Driessche, J., 2003. How plausible are high-frequency sediment supply-driven cycles in the stratigraphic record? Sedimentary Geology 157, 3–13, doi:10.1016/S0037-0738(03)00066-6.

667 Castillo, V.M., Martinez-Mena, M., Albaladejo, J., 1997. Runoff and soil loss response to vegetation removal in
668 a semiarid environment. Soil Sci. Soc. Am. J. 61, 1116 – 1121,
669 doi:10.2136/sssaj1997.03615995006100040018x.
670 Clapp, E.M., Bierman, P.R, Nichols, K.K., Pavich, M., Caffee, M., 2001. Rates of sediment supply to arroyos
671 from upland erosion determined using in situ produced cosmogenic ^{10}Be and ^{26}Al. Quaternary Research
672 55, 235–245.
673 Cochonat, P., 1998. ZAIANGO2 cruise, L'Atalante R/V. doi:10.17600/98010110
674 Cochonat, P., Robin, A., 1992. GUINESS I cruise, L'Atalante R/V. doi:10.17600/92004211
675 Coulter, G.W., 1991. Lake Tanganyika and its life. Oxford Univ. Press, New York.
676 Coynel, A., Seyler, P., Etcheber, H., Meybeck, M., Orange, D., 2005. Spatial and seasonal dynamics of total
677 suspended sediment and organic carbon species in the Congo River. Global biogeochemical cycles 19,
678 GB4019.
679 Crétaux, J.-F., Jelinski, W., Calmant, S., Kouraev, A., Vuglinski, V., Bergé-Nguyen, M., Gennero, M.-C., Nino,
680 F., Abarca Del Rio, R., Cazenave, A., Maisongrande, P., 2011. SOLS: A lake database to monitor in the
681 Near Real Time water level and storage variations from remote sensing data. Advance in Space Research
682 47, 1497-1507.
683 Crippen, R.E., 1990. Calculating the vegetation index faster, Remote Sensing of Environment 34, 71-73.
684 De Namur, C., 1990. Aperçu sur la végétation de l'Afrique Centrale Atlantique. in Lanfranchi R., Schwartz, D.
685 (eds). Paysages Quaternaires de l'Afrique Centrale Atlantique, Inst. Fr. de Rech. Sci. pour le Dev. en
686 Coop. (ORSTOM), Paris.
687 De Vente, J., Poesen, J., 2005. Predicting soil erosion and sediment yield at the basin scale: scale issues and
688 semi-quantitative models. Earth-Science Reviews 71, 95-125.
689 Dalibard, M., Popescu, S.-M., Maley, J., Baudin, F., Melinte-Dobrinescu, M.-C., Pittet, B., Marsset, T.,
690 Dennielou, B., Droz, L., Suc, J.-P., 2014. High-resolution vegetation history of West Africa during the
691 last 145 ka. Geobios 47, 183–198. doi:10.1016/j.geobios.2014.06.002
692 Droz, L., Marsset, T., 2011. REPREZAI_LEG2 cruise, Le Suroît R/V,. doi:10.17600/11020020
693 Droz, L., Marsset, T., Ondréas, H., Lopez, M., Savoye, B., Spy-Anderson, F.-L., 2003. Architecture of an active
694 mud-rich turbidite system: The Zaire Fan (Congo–Angola margin southeast Atlantic). Results from
695 ZaïAngo 1 and 2 cruises. AAPG Bull. 87, 1145–1168. doi:10.1306/03070300013
696 Dunne, T., 1979. Sediment yield and land use in tropical catchments. Journal of Hydrology 42, 281-300.
697 Elenga,H., Maley, J., Vincens, A., Farrera, I., 2004. Palaeoenvironments, Palaeoclimates and Landscape
698 development in Atlantic equatorial Afraica: a review of key sites covering the last 25 kyrs. In Battarbee
699 R.W. et al. (eds), Past Climate Variability through Europe and Africa. Kluwer Academic Publishers,
700 Dordrecht, The Netherlands, 181-198.
701 El-Hassanin, A.S., Labib, T.M., Gaber, E.I., 1993. Effect of vegetation cover and land slope on runoff and soil
702 losses from the watersheds of Burundi. Agriculture, Ecosystems and Environment 43, 301-308.
703 El Kateb, H., Zhang, H., Zhang, P., Mosandl, R., 2013. Soil erosion and surface runoff on different vegetation
704 covers and slope gradients: a field experiment in Southern Shaanxi Province, China. Catena 105, 1-10.
705 Ellis, E.E., Keil, R.G., Ingalls, A.E., Richey, J.E., Alin, S.R., 2012. Seasonal variability in the sources of
706 particulate organic matter of the Mekong River as discerned by elemental and lignin analyses. J.
707 Geophys. Res. 117, G01038, doi:10.1029/2011JG00.
708 Farr, T.G., Rosen, P.A., Caro, E., Crippen, R., Duren, R., Hensley, S., Kobrick, M., Paller, M., Rodriguez, E.,
709 Roth, L., Seal, D., Shaffer, S., Shimada, J., Umland, J., Werner, M., Oskin, M., Burbank, D.W., Alsdorf,
710 D., 2007. The Shuttle radar topography mission. Reviews of Geophysics 45, RG2004.
711 Flügel, T.J., Eckardt, F.D., Cotterill, F.P.D., 2015. The present day drainage patterns of the Congo river system
712 and their Neogene evolution. in: M.J. de Wit et al. (eds.), Geology and Resource Potential of the Congo
713 Basin, Regional Geology Reviews, Springer-Verlag Berlin Heidelberg. DOI 10.1007/978-3-642-29482-
714 2_15
715 Gaillardet, J., Dupré, B., Allègre, C.J., 1995. A global chemical budget applied to the Congo basin rivers:
716 Erosion rates and continental crust composition, Geochim. Cosmochim. Acta 59, 3469 – 3485.
717 Gent, P.R., Danabasoglu, G., Donner, L.J., Holland, M.M., Hunke, E.C., Jayne, S.R., Lawrence, D.M., Neale,
718 I.B., Rasch, P.J., Vertenstein, M., Worley, P.H., Yang, Z.-L., Zhang, M., 2011. The Community Climate
719 System Model Version 4. Journal of Climate 24, 4973-4991.

Gingele, F.X., Müller, P.M., Schneider, R.R., 1998. Orbital forcing of freshwater input in the Zaire Fan area - clay mineral evidence from the last 200 kyr. Palaeogeogr. Palaeoclimatol. Palaeoecol. 138, 17–26. doi:10.1016/S0031-0182(97)00121-1

Giresse, P., Wiewiora, A., Lacka, B., 1988. Mineral phases and processes within green peloids from two recent deposits near the Congo River mouth. Clay Minerals 23, 447–458.

GRDC, Global Runoff Data Center, 2016. http://www.bafg.de/GRDC/EN/Home/homepage_node.html (last accessed October 2016).

Govin, A., Holzwarth, U., Heslop, D., Ford Keeling, L., Zabel, M., Mulitza, S., Collins, J.A., Chiessi, C.M., 2012. Distribution of major elements in Atlantic surface sediments (36°N–49°S): Imprint of terrigenous input and continental weathering. Geochem. Geophys. Geosystems 13, Q01013. doi:10.1029/2011GC003785

Guillocheau, F., Chelalou, R., Linol, B., Dauteuil, O., Robin, C., Mvondo, F., Callec, Y., Colin, J.-P., 2015. Cenozoic Landscape Evolution in and Around the Congo Basin: Constraints from Sediments and Planation Surfaces. in: M.J. de Wit et al. (eds.), Geology and Resource Potential of the Congo Basin, Regional Geology Reviews, Springer-Verlag Berlin Heidelberg. DOI 10.1007/978-3-642-29482-2_14

Guillocheau, F., Galmier, V., Robin, C., 2016. Source to Sink study of the Congo system since 40 Myr: a measurement ratio between mechanical and chemical erosion. *In* "Source to Sink: a long term perspective of sediment budgets and sources characterization" meeting, Nov 2016, Rennes, France. Abstracts book, p.62.

Gyssels, G., Poesen, J., Bochet, E., Li, Y., 2005. Impact of plant roots on the resistance of soils to erosion by water: a review, Prog. Phys. Geogr., 29(2), 189 – 217.

Hardy, W., Penaud, A., Marret, F., Bayon, G., Marsset, T., Droz, L., 2016. Dinocyst assemblage constraints on oceanographic and atmospheric processes in the eastern equatorial Atlantic over the last 44 kyr. Biogeosciences 13, 4823–4841. http://dx.doi.org/10.5194/bg-13-4823-2016.

Hatin, T., Crosta, X., Le Hérissé, A., Droz, L., Marsset, T., 2017. Diatom response to oceanographic and climatic changes in the Congo fan area, equatorial Atlantic Ocean, during the last 190 ka BP. Palaeogeogr., Palaeoclimato., Palaeoecol. 469, 47-59.

Hijmans, R.J., Cameron, S.E., Parra, J.L., Jones, P.G., Jarvis, A., 2005. Very high resolution interpolated climate surfaces for global land areas. International Journal of Climatology 25, 1965–1978.

Huete, A., Disan, K., Miura, T., Rodriguez, E.P., Gao, X., Ferreira, L.G., 2002. Overview of the radiometric and biophysical performance of the MODIS vegetation indices. Remote Sensing of Environment 83, 195-213.

HYBAM, 2016. Contrôles géodynamique, hydrologique et biogéochimique de l'érosion/altération et des transferts de matière dans les bassins de l'Amazone, de l'Orénoque et du Congo. Available at http://www.ore-hybam.org, (last accessed Nov. 2016).

Jolly, D., Harrison, S.P., Damnati, B., Bonnefille, R., 1998. Simulated climate and biomes of Africa during the Qauternary: comparison with pollen and Lake Status data. Quaternary Science Reviews 17, 629-657.

Jung, H.K., Hamski, J., Durand, M., Alsdorf, D., Hossain, F., Lee, H., Azad Hossain, A.K.M., Hasan, K., Saleh A., Khan, Zeaul Hoque, A.K.M., 2010. Characterization of complex fluvial systems using remote sensing of spatial and temporal water level variations in the Amazon, Congo, and Brahmaputra Rivers, Earth Surface Processes and Landforms 35, 294 –304, doi:10.1002/esp.1914.

Kettner, A.J., Syvitski, J.P.M., 2008. HydroTrend v. 3.0: A climate-driven hydrological transport model that simulates discharge and sediment load leaving a river system. Computers & Geosciences 34 (10), 1170-1183.

Kettner, A.J., Syvitski, J.P.M., 2009. Fluvial responses to environmental perturbations in the Northern Mediterranean since the Last Glacial Maximum. Quaternary Science Reviews 28 (23), 2386-2397.

Kinga-Mouzeo, 1986. Transport particulaire actuel du fleuve Congo et de quelques affluents; enregistrement quaternaire dans l'éventail détritique profond (sédimentologie, minéralogie et géochimie). PhD thesis, Université de Perpignan. 251 pp.

Kottek, M., Grieser, J., Beck, C., Rudolf, B., Rubel, F., 2006. World Map of the Köppen-Geiger climate classification updated. Meteorologische Zeitschrift 15(3), 259-263.

Kutzbach, J., Gallimore, R., Harrison, S., Behling, P., Selin, R., Laarif, F., 1998. Climate and Biome simulations for the past 21,000 years. Quaternary Science Reviews 17, 473-506.

Lal, R., 1985. Soil erosion and sediment transport research in tropical Africa. Hydrological Sciences Journal 30 (2), 239-256. DOI: 10.1080/02626668509490987

Laraque, A., Bricquet, J.P., Berthelot, M., Olivry, J.C., 1995. Aspects hydrologiques du fleuve Congo. Proceeding of PEGI international meeting 22-44 may 1993, CNRS-INSU-ORSTOM, Paris.

Laraque, A., Orange, D., 1996. Banque de données hydrochimiques des eaux de surfaces d'Afrique Centrale (Congo et Oubangui) de 1987 à 1994. Programme PEGI-GBF, ORSTOM, Montpellier. 145 pp.

Laraque, A., Pouyaud, B., Rocchia, R., Robin R., Chaffaut I., Moutsambote, J.-M., Maziezoula, B., Censier, C., Albouy, Y., Elenga, H., Etcheber, H., Delaune, M., Sondag, F., Gasse, F., 1998. Origin and function of a closed depression in equatorial humid zones: the lake Tele in north Congo. Journal of Hydrology 207, 236–253.

Laraque, A., Bricquet, J.P., Pandi, A., Olivry, J.C., 2009. A review of material transport by the Congo river and its tributaries. Hydrological Processes 23, 3216-3224.

Laraque, **A.,** Bellanger, M., Adele, G., Guebanda, S., Gulemvuga, G., Pandi, A., Paturel, J.E., Robert, A., Tathy, J.P., Yambele A.. 2013a. Evolutions récentes des débits du Congo, de l'Oubangui et de la Sangha. 2013a. Geo-Eco-Trop. 37(1), 93-100.

Laraque, A., Castellanos, B., Steiger, J., Lòpez, J.L., Pandi, A., Rodriguez, M., Rosales, J., Adèle, G., Perez, J., Lagane, C., 2013b. A comparison of the suspended and dissolved matter dynamics of two large inter-tropical rivers draining into the Atlantic Ocean: the Congo and the Orinoco. Hydrol. Process. 27, 2153–2170. doi:10.1002/hyp.9776

Latham, J., Cumani, R., Rosati, I., Bloise, M., 2014. Global Land Cover SHARE (GLC-SHARE) database Beta-Release Version 1.0. Rome: FAO. Accessed March 27. http://www.glcn.org/downs/prj/glcshare/GLC_SHARE_beta_v1.0_2014.pdf

Latrubesse, E.M., Arima, E.Y., Dunne, T., Park, E., Baker, V.R., d'Horta, F.M., Wight, C., Wittmann, F., Zuanon, J., Baker, P.A., Ribas, C.C., Norgaard, R.B., Filizola, N., Ansar, A., Flyvbjerg B., and Stevaux J.C., 2017. Damming the rivers of the Amazon basin. Nature 546, 363–369 doi:10.1038/nature22333

Laurent D., Picot M., Marsset T., Droz L., Rabineau M., Granjeon D., Molliex S., 2017. 3D stratigraphic modeling of the Congo turbidite system since 210 ka: an investigation of factors controlling sedimentation. EGU General Assembly, 23-28 April 2017, Vienna, Austria, Vol. 19, 08963.

Lee, H., Beighley, R.E., Alsdorf, D., Jung, H.-C., Shum, C.K., Duan, J., Guo, J., Yamazaki, D., Andreadis, K., 2011. Characterization of terrestrial water dynamics in the Congo Basin using GRACE and satellite radar altimetry, Remote Sens. Environ. 115, 3530–3538, doi:10.1016/j.rse.2011.08.015.

Lee, H., Jung, H.C., Yuan, T., Beighley, R.E., Duan, J., 2014. Controls of terrestrial water storage changes over the central Congo Basin determined by integrating PALSAR ScanSAR, Envisat altimetry, and GRACE data, in Remote Sensing of the Terrestrial Water Cycle, AGU Geophys. Monogr. 206, edited by V. Lakshmi et al., pp. 117–129, John Wiley, Hoboken, N.J., doi:10.1002/9781118872086.

Lee, H., Yuan, T., Jung, H.C., Beighley, E., 2015. Mapping wetland water depths over the central Congo Basin using PALSAR ScanSAR, Envisat altimetry, and MODIS VCF data, Remote Sens. Environ. 159, 70–79.

Leturmy, P., Lucazeau, F., Brigaud, F., 2003. Dynamic interactions between the Gulf of Guinea passive margin and the Congo River drainage basin: 1. Morphology and mass balance. J. Geophys. Res. 108(B8), 2383, doi:10.1029/2002JB001927.

Leopold, L.B., Maddock, T., 1953. The Hydraulic Geometry of Stream Channels and Some Physiographic Implications. U.S. Geological Survey Professional Paper 252.

Lisiecki, L.E., Raymo, M.E., 2005. A Pliocene-Pleistocene stack of 57 globally distributed benthic δ18O records. Paleoceanography 20, PA1003. doi:10.1029/2004PA001071

Maley, J., 1982. Dust, clouds, rain types and climatic variations in tropical North Africa. Quat. Res. 18, 1-16.

Maley, J., 1992. Mise en évidence d'une péjoration climatique entre ca. 2 500 et 2000 ans BP en Afrique tropicale humide. Bull. Soc. Géol. France 163, 363-365.

Maley, J., Brenac, P., Bigot, S., Moron, V., 2000. Le domaine forestier africain et ses marges : les transitions climatiques majeures à l'époque actuelle et au cours des derniers millénaires. In Servant, M., Servant-Vildary, S. (eds). Dynamique à long terme des écosystèmes forestiers intertropicaux, chapter 25, UNESCO.

Maley, J., Giresse, P., Doumenge, C., Favier, C., 2012. Comment on "Intensifying Weathering and Land Use in Iron Age Central Africa." Science 337, 1040–1040. doi:10.1126/science.1221820

Marsset, T., Droz, L., 2010. REPREZAI_LEG1 cruise, Pourquoi Pas? R/V. doi:10.17600/10030170
Marsset, T., Droz, L., Dennielou, B., Pichon, E., 2009. Cycles in the architecture of the Quaternary Zaïre turbidite system: a possible link with climate. Extern. Controls Deep-Water Depositional Syst. 89–106.
Martins, O., Probst, J.L., 1991. Biogeochemistry of major African rivers: Carbon and minerals transport, in Degens, E.T., Kempe, S., Richey J.E. (eds). Biogeochemistry of Major World Rivers. SCOPE 42, 127–156.
Métivier, F., Gaudemer, Y., 1999. Stability of output fluxes of large rivers in South and East Asia during the last 2 million years: Implications on floodplain processes. Basin Research 11, 293–303, doi:10.1046/j.1365-2117.1999.00101.x
Matmon, A., Bierman, P.R., Larsen, M.C., Southworth, S., Pavich, M., Caffee, M., 2003. Temporally and spatially uniform rates of erosion in the southern Appalachian Great Smoky Mountains. Geology 31, 155–158.
Meybeck, M., 2003. Global analysis of river systems: from Earth system controls to Anthropocene controls. Phil. Trans. R. Soc. B 358, 1935–1955.
Michalopoulos, P., Aller, R.C., 2004. Early diagenesis of biogenic silica in the Amazon delta : Alteration, authigenic clay formation, and storage. Geochimica and Cosmochimica Acta 68, 1061-1085.
Morehead, M.D., Syvitski, J., Hutton, E.W.H., Peckham, S.D., 2003. Modeling the temporal variability in the flux of sediment from ungauged river basins. Global and Planetary Change 39, 95-110.
Morin-Rivat, J., Fayolle, A., Gillet, J.-F., Bourland, N., Gourlet-Fleury, S., Oslisly, R., Bremond, L., Bentaleb, I., Beeckman, H., Doucet, J.-L., 2014. New evidence of human activities during the Holocene in the lowland forests of the northern Congo basin. Radiocarbon 56(1), 209-220.
Neumann, J., 1955. Latitudinal variation of tropospheric temperature lapse rate. Archiv für Meteorologie, Geophysik und Bioklimatologie, Serie A 8(4), 351-353.
Neumann, K., Eggert, M.K.H., Oslisly, R., Clist, B., Denham, T., Maret, P. de, Ozainne, S., Hildebrand, E., Bostoen, K., Salzmann, U., Schwartz, D., Eichhorn, B., Tchiengué, B., Höhn, A., 2012. Comment on "Intensifying Weathering and Land Use in Iron Age Central Africa." Science 337, 1040–1040. doi:10.1126/science.1221747
Nkounkou, R.R., Probst, J.L., 1987. Hydrology and geochemistry of the Congo River system. In Degens E.T. et al. (eds). Transport of Carbon and Minerals in Major World Rivers, Part 4. Mitt. Geol-Paläont. Insti. Univ. Hambourg, SCOPE/UNEP Sond. 64, 483-508.
O'Loughlin, F., Trigg, M.A., Schumann, G.J.P., Bates, P.D., 2013. Hydraulic characterization of the middle reach of the Congo River, Water Resource Research 49, 5059–5070, doi:10.1002/wrcr.20398.
Osmaston, H.A., Harrison, S.P., 2005. Quaternary glaciations of Africa: A regional synthesis. Quaternary International 138-139, 32-54.
Peckham, S.D., 2009. Geomorphometry in RiverTools, In: Hengl, T., Reuter, H.I. (eds), Geomorphometry: Concepts, Software and Applications, Chapter 18, Developments in Soil Science 33, 411-430.
Pelletier, J.D., 2012. A spatially distributed model for the long-term suspended sediment discharge and delivery ratio of drainage basins. Journal of Geophysical Research 117, F02028, doi:10.1029/2011JF002129
Phillips, J.D., 2003. Alluvial storage and the long-term stability of sediment yields. Basin Research 15(2), 153–163, doi: 10.1046/j.1365-2117.2003.00204.x.
Picot, M., 2015. Cycles sédimentaires dans le système turbiditique ud Congo : nature et origine. PhD thesis, Université de Bretagne Occidentale, Brest. 368 pp.
Picot, M., Droz, L., Marsset, T., Dennielou, B., Bez, M., 2016. Controls on turbidite sedimentation: Insights from a quantitative approach of submarine channel and lobe architecture (Late Quaternary Congo Fan). Marine and Petroleum Geology 72, 423-446.
Picouet, C., Hingray, B., Olivry, J.C., 2001. Empirical and conceptual modelling of the suspended sediment dynamics in a large tropical African river: the Upper Niger River basin. Journal of Hydrology 250, 19-39.
Rabouille, C., Caprais, J.-C., Lansard, B., Crassous, P., Dedieu, K., Reyss, J.-L., Khripounoff, A., 2009. In situ measurements of sediment oxygen consumption and organic matter budget in the Southeast Atlantic continental margin close to the Congo Canyon. Deep Sea Research Part II 56, 2223–2238.
Regard, V., Carretier, S., Boeglin, J.-L., Ndam Ngoupayou, J.-R., Dzana, J.-G., Bedimo Bedimo, J.-P., Riotte, J., Braun, J.-J., 2016. Denudation rates on cartonic landscapes: comparison between suspended and

dissolved fluxes, and 10Be analysis in the Nyong ans Sanaga River basins, south Cameroon. Earth Surface Processes and Landforms 41, 1671-1683. doi: 10.1002/esp.3939

Reichenstein, M., Bahn, M., Ciais, P., Frank, D., Mahecha, M.D., Seneviratne, S.I., Zscheischler, J., Beer, C., Buchmann, N., Frank, D.C., Papale, D., Rammig, A., Smith, P., Thonicke, K., van der Velde, M., Vicca, S., Walz, A., Wattenbach, M., 2013. Climate extremes and the carbon cycle. Nature 500, 287-295.

Rodier, J., 1964. Régimes hydrologiques de l'Afrique Noire à l'Ouest du Congo. Mem. ORSTOM 6, 137 pp.

Rogers, R.D., Schumm S.A., 1991. The effect of sparse vegetative cover on erosion and sediment yield, J. Hydrol. 123, 19 – 24. doi:10.1016/0022-1694(91)90065-P.

Roller, S., Wittmann, H., Kastowski, M., Hinderer, M., 2012. Erosion of the Rwenzori Mountains, East African Rift, from in situ-produced cosmogenic 10Be. Journal of Geophysical Research 117, F03003. DO I: 10.1029/2011JF002117

Rommerskirchen, F., Eglinton, G., Dupont, L., Rullkötter, J., 2006. Glacial/interglacial changes in southern Africa: Compound-specific d13C land plant biomarker and pollen records from southeast Atlantic continental margin sediments. Geochem. Geophys. Geosyst. 7, Q08010. doi:10.1029/2005GC001223.

Savoye, B., 1998. ZAIANGO1 cruise, L'Atalante R/V. doi:10.17600/98010100

Savoye, B., Babonneau, N., Dennielou, B., Bez, M., 2009. Geological overview of the Angola–Congo margin, the Congo deep-sea fan and its submarine valleys. Deep Sea Res. Part II Top. Stud. Oceanogr. 56, 2169–2182. doi:10.1016/j.dsr2.2009.04.001

Schneider, R.R., Price, B., Müller, P.J., Kroon, D., Alexander, I., 1997. Monsoon related variations in Zaire (Congo) sediment load and influence of fluvial silicate supply on marine productivity in the east equatorial Atlantic during the last 200,000 years. Paleoceanography 12, 463–481. doi:10.1029/96PA03640

Sichingabula, H.M., (1999). Special study on sediment discharge and its consequence: analysis and results of discharge and sediment monitoring activities in the southern Lake Tanganyika basin, Zambia. Technical report number 4. UNDP/GEF. Dar es Salaam, Tanzania, 106 pp.

Simpson, G., Castelltort, S., 2012. Model shows that rivers transmit high-frequency climate cycles to the sedimentary record. Geology 40(12), 1131-1134. doi:10.1130/G33451.1

Sionneau, T., Droz, L., Marsset, T., Dennielou, B., Bez, M., 2010. Congo-Zaire detrital supply variability during the last 200 ka: a possible explanation for the longitudinal migration of the Zaire fan depocenters. 18th International Sedimentological Congress, 26/09 to 01/10 2010, Mendoza (Argentine).

Spencer, R.G.M., Hernes, P.J., Dinga, B., Wabakanghanzi, J.N., Drake, T.W., Six, J., 2016. Origins, seasonality, and fluxes of organic matter in the Congo River, Global Biogeochem. Cycles 30, doi:10.1002/2016GB005427.

Summerfield, M.A., Hulton, N.J., 1994. Natural controls of fluvial denudation rates in major world drainage basins. J. Geophys. Res. Solid Earth 99, 13871–13883. doi:10.1029/94JB00715

Syvitski, J.P.M., Morehead, M.D., Nicholson, M., 1998. Hydrotrend: a climate-driven hydrologic-transport model for predicting discharge and sediment load to lakes or oceans. Computers & Geosciences 24, 51-68.

Syvitski, J.P.M., Morehead, M.D., 1999. Estimating river-sediment discharge to the ocean: application to the Eel margin, North California. Marine Geology 154,13–28.

Syvitski, J.P.M., Milliman, J., 2007. Geology, geography, and humans battle for dominance over the delivery of fluvial sediment to the coastal ocean. The Journal of Geology 115, 1–19.

Syvitski, J.P.M., Morehead, M.D., Bahr, D.B., Mulder, T., 2000. Estimating fluvial sediment transport: The rating parameters. Water Resources Research 36(9), 2747-2760.

Syvitski, J.P.M., Morehead, M.D., Nicholson, M., 1998. HydroTrend: a climate-driven hydrologic-transport model for predicting discharge and sediment load to lakes or the ocean. Comput Geosci 24(1), 51–68.

Syvitski, J.P.M., Vörösmarty, C.J., Kettner, A.J., Green, P., 2005. Impact of humans on the flux of terrestrial sediment to the global coastal ocean. Science 308, 376-380.

Syvitski, J.P.M., Kettner, A.J., Overeem, I., and Brakenridge, G.R., 2017. Latitudinal controls on siliciclastic sediment production and transport. SEPM Special Publication No. 108. Doi: http://dx.doi.org/10.2110/sepmsp.108.04.

Thiry, M., 2000. Paleoclimatic interpretation of clay minerals in marine deposits: an outlook from the continental origin. Earth Science Review 49, 201–221.

Tucker, C.J., 1979. Red and Photographic Infrared Linear Combinations for Monitoring Vegetation, Remote Sensing of Environment 8(2),127-150.

Vance, D., Bickle, M., Ivy-Ochs, S., Kubik, P.W., 2003. Erosion and exhumation in the Himalaya from cosmogenic isotope inventories of river sediments. Earth and Planetary Science Letters 206, 273–288.

Vangriesheim, A., Pierre, C., Aminot, A., Metzl, N., Baurand, F., Caprais, J.C., 2009. The influence of Congo River discharges in the surface and deep layers of the Gulf of Guinea, Deep Sea Research Part II 56, 2183–2196.

Vanmaercke, M., Poesen, J., Broeckx, J., Nyssen, J., 2014. Sediment Yield in Africa. Earth-Science Reviews 136, 350-368. doi: 10.1016/j.earscirev.2014.06.004

Vörösmarty C.J., Meybeck, M., Fekete, B., Sharma, K., 1997. The potential impact of neo-Castorization on sediment transport by the global network of rivers. In: Walling D., Probst, J.L. eds., Human Impact of erosion and sedimentation. IAHS Press, Wallingford, UK., 261–272.

Walling, D.E., 2006. Human impact on land–ocean sediment transfer by the world's rivers. Geomorphology 79, 192–216.

Wang, J.-J., Adler, R.F., Huffman, G.J., Bolvin, D., 2014. An updated TRMM composite climatology of tropical rainfall and its validation. J. Climate 27, 273-284.

Weijers, J.W.H., Schefuss, E., Schouten, S., Sinninghe Damsté J.S., 2007. Coupled Thermal and Hydrological Evolution of Tropical Africa over the Last Deglaciation. Science 315, 1701-1704. doi: 10.1126/science.1138131.

Weldeab, S., Lea, D.W., Schneider, R.R., Andersen. N., 2007. 155,000 Years of West African Monsoon and Ocean Thermal Evolution. Science 316, 1303-1307. doi: 10.1126/science.1140461

Wilby, R.L., Dalgleish, H.Y., Foster, I.D.L., 1997. The impact of weather patterns on historic and contemporary catchment sediment yields. Earth Surface Processes and Landforms 22, 353–63.

Winemiller, K.O. et al., 2016. Balancing hydropower and biodiversity in the Amazon, Congo and Mekong. Science 351, 128–129.

Wittmann, H., von Blanckenburg, F., Maurice, L., Guyot, J.-L., Filizola, N., Kubik, P.W., 2011. Sediment production and delivery in the Amazon River basin quantified by in situ-produced cosmogenic nuclides and recent river loads. GSA bulletin 123(5-6), 934-950. doi: 10.1130/B30317.1

Wotzka, H.P., 2006. Records of activity: radiocarbon and the structure of Iron Age settlement in Central Africa. In: Wotzka, H.P., ed. Grundlegungen. Beiträgezur europäischen und afrikanischen Archäologie für Manfred K.H. Eggert. Tübingen: Francke Attempto Verlag, 271–289.

Xie, Y., Sha, Z., Yu, M., 2008. Remote sensing imagery in vegetation mapping: a review. Journal of Plant Ecology 1(1), 9-23.

Xu, J.X., 2003. Sediment flux to the sea as influenced by changing human activities and precipitation: example of the Yellow River, China. Journal of Environmental Management 31(3), 328–41.

Zomer, R.J., Trabucco, A., Bossio, D.A., Verchot, L.V., 2008. Climate change mitigation: A spatial analysis of global land suitability for clean development mechanism afforestation and reforestation. Agriculture Ecosystems and Environment 126, 67-80.

Zhang, Q., Justice, C.O., Jiang, M., Brunner, J., Wilkie, D.S., 2006. A GIS-based assessment on the vulnerability and future extent of the tropical forests of the Congo basin. Environmental Monitoring and Assessment 114, 107-121.

Zhu, Y.M., Lu, X.X., Zhou, Y., 2007. Suspended sediment flux modeling with artificial neural network: an example of the Longchuanjiang River in the upper Yangtze catchment, China. Geomorphology 84,111–125.

Figures

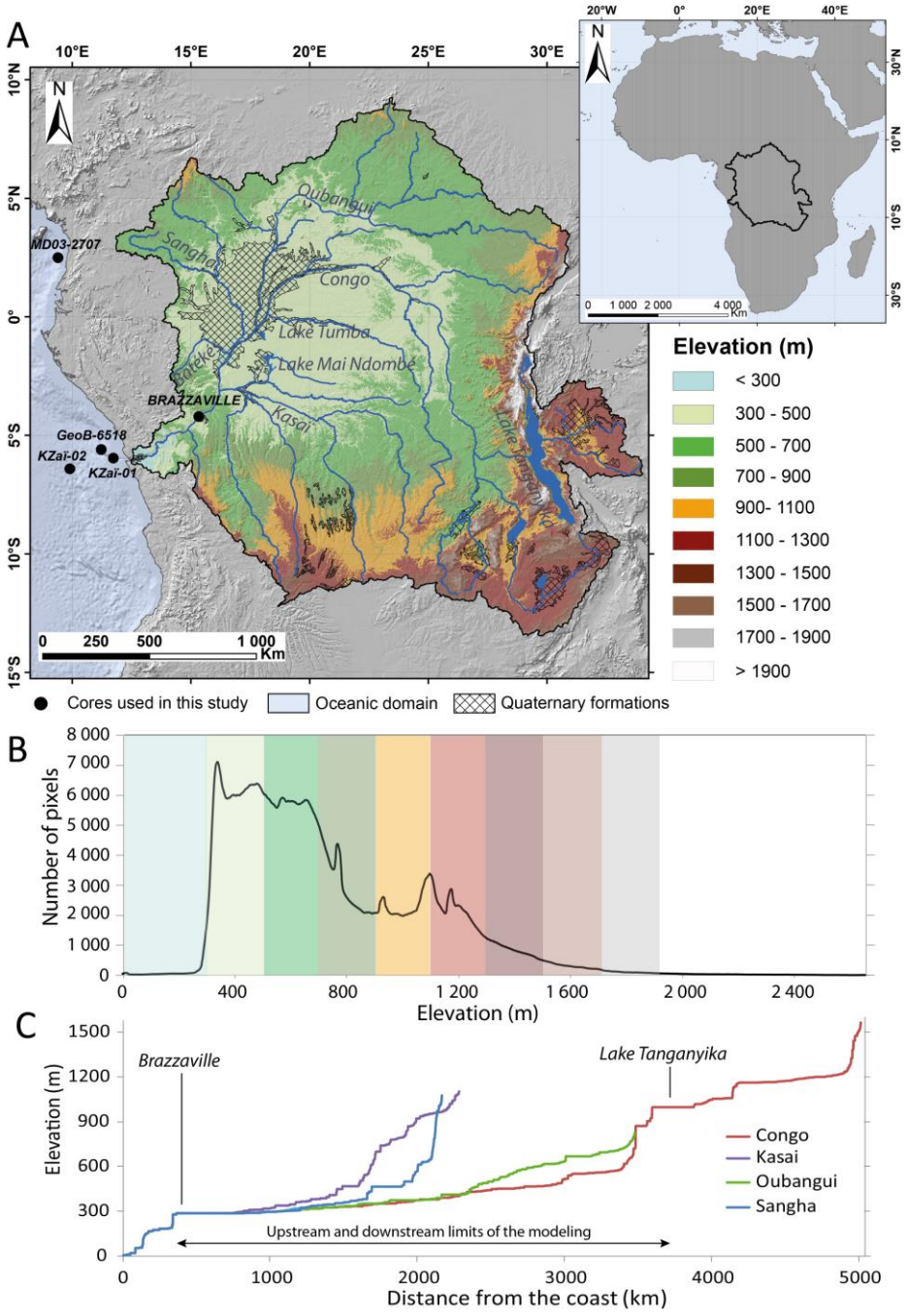

Figure 1: Geomorphological setting of the Congo catchment. A) Drainage basin represented by elevation, where dark blue indicates the Congo River with its major tributaries and lakes, location of datasets used and Quaternary deposits. B) Statistical distribution of elevation within the catchment. C) Longitudinal profiles of the Congo River and its main tributaries, with upstream and downstream boundaries of the modeling. Note that the knickpoint on the Congo River profile at Brazzaville indicates that regressive erosion due to the successive marine oscillations in Quaternary does not affect the morphology of the catchment above this point.

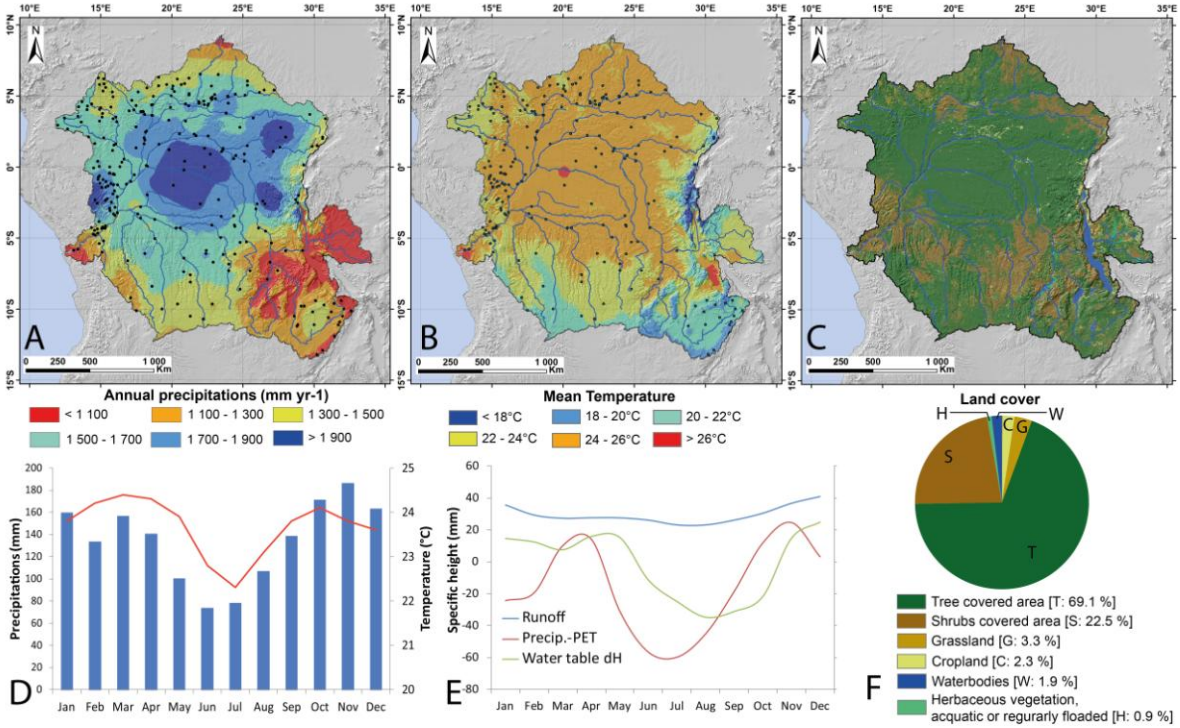

Figure 2: Environmental setting of the Congo catchment. A) Spatial distribution of annual precipitations (data from Hijmans et al., 2005) and location of the SIEREM stations used for calculation of temporal precipitation standard variation. B) Spatial distribution of mean annual temperature (data from Hijmans et al., 2005). C) Spatial distribution of land cover (data from Latham et al., 2014). D) Mean monthly precipitations (blue bars) and temperature (red line). E) Monthly water balance, with runoff (blue) (data from Laraque et al., 2013), available water (precipitation minus potential evapo-transpiration (PET; Zomer et al., 2008, in red) and variations in water table height (from lakes-level satellite-monitoring; Crétaux et al., 2011; Becker et al., 2014, in green). F) Quantitative repartition of land cover.

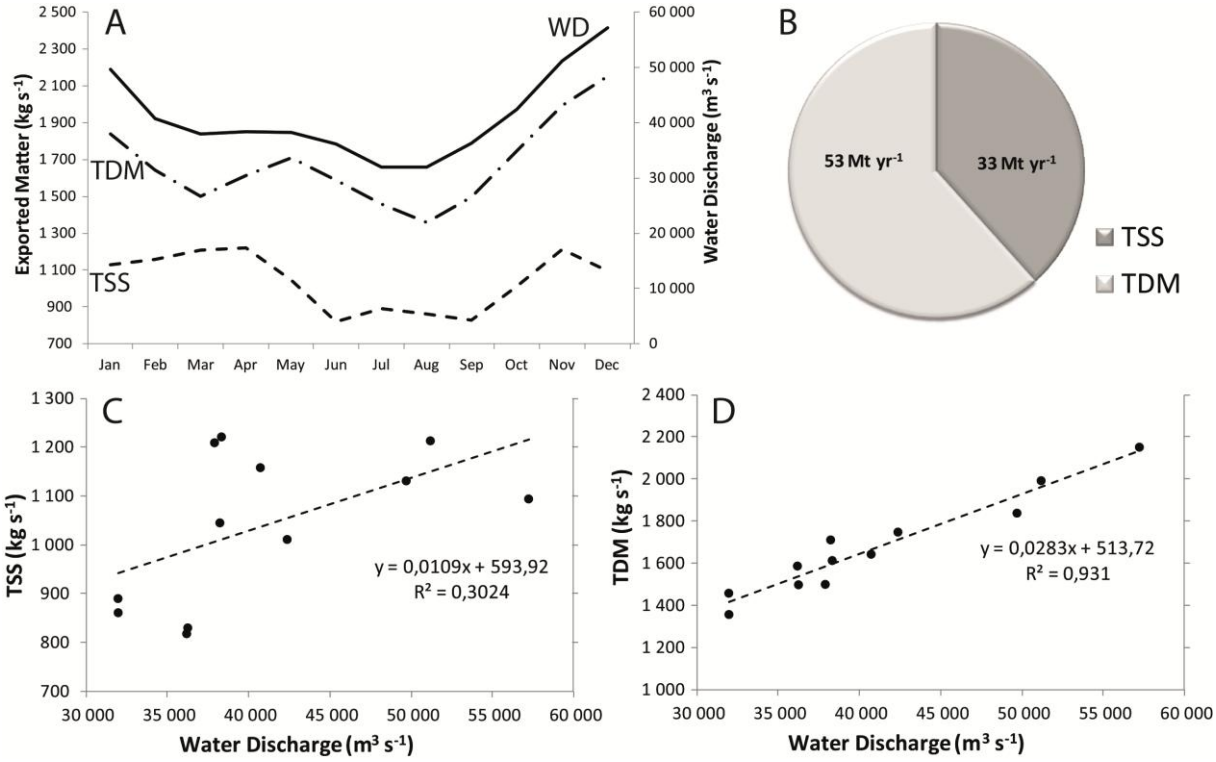

995

996 Figure 3: Mean monthly water and sediment discharge of the Congo watershed, in-situ monitored at
997 Brazzaville gauging station (from Laraque et al., 2013). A) Monthly water discharge (WD; solid line),
998 monthly Total Suspended Sediments (TSS; regular-dashed line), monthly Total Dissolved Matter
999 (TDM, dashed line with dots). B) Annual sediment yield (Total Suspended Sediments and Total
1000 Dissolved Matter, respectively) exported from the Congo catchment. C) Relation between mean
1001 monthly TSS and mean monthly water discharge. D) Relation between mean monthly TDM and mean
1002 monthly water discharge.

1003

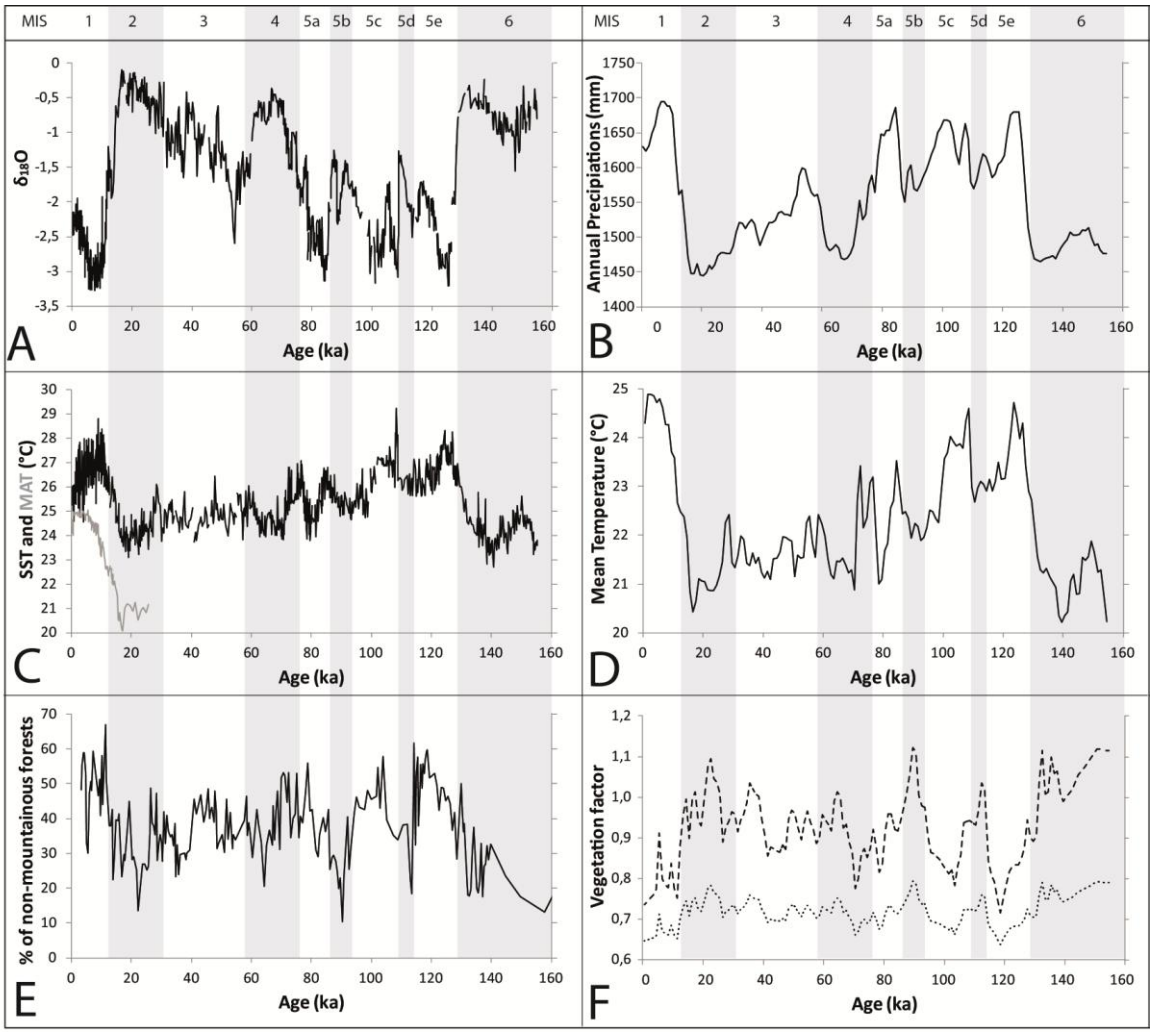

Figure 4: Evolution of different marine proxies over the last 155 ka (A, C, E), used for the interpretation of environmental changes (B, D, F). A) $\delta^{18}O$ curve of the MD03-2707 core which is located in the Guinea Gulf (Weldeab et al., 2007). B) Interpretation of $\delta^{18}O$ data in terms of precipitation changes, since these data are interpreted as representative of the monsoon intensity (Weldeab et al., 2007; Caley et al., 2011). C) Sea Surface Temperature curve (SST, black line) of the MD03-2707 core (Weldeab et al., 2007) and Mean Atmospheric Temperature (MAT, grey line) of the GeoB6518-1 core (Weijers et al., 2007). D) Interpretation of SST and MAT in terms of mean catchment temperatures. For B and D, the calibration is performed to present-day (Hijmans et al., 2005) and the LGM (Gent et al., 2011) from global climatic model CCSM4 values and the data are smoothed by applying a mean value for: i) a 1 ka step for the 155 ka simulation, and ii) a 200 years step for the 23 ka simulation. E) Percentage of non-mountainous forests pollens for the KZaï-02 core (Dalibard et al., 2014). F) Interpretation of non-mountainous forests pollens in terms of vegetation factor (method detailed in text). The dotted line represents the minimum value and the dashed line the maximum.

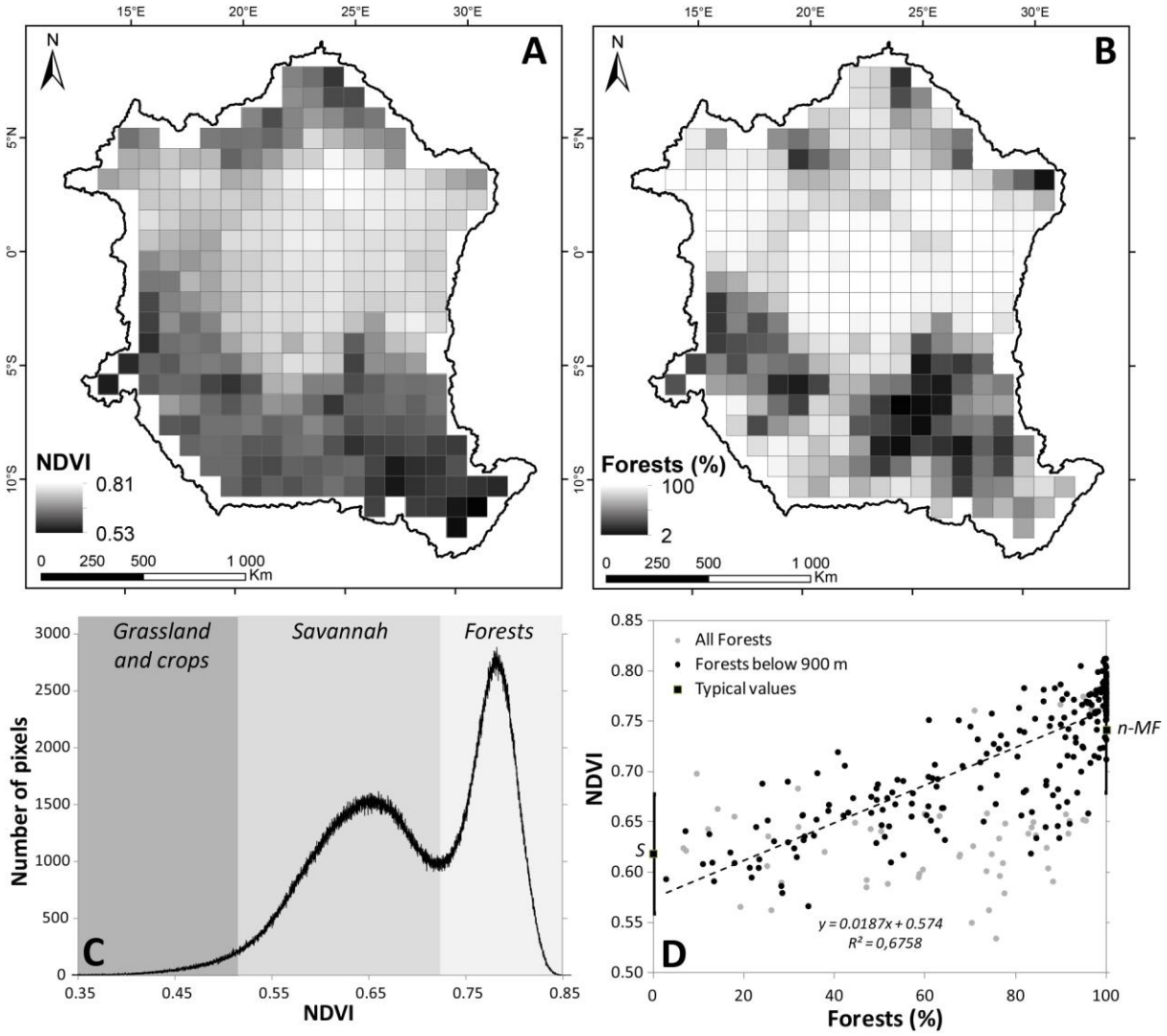

Figure 5: The relation between NDVI (Normalized Difference Vegetation Index) and spatial Forest distribution. A) Mean annual NDVI averaged for 100 x 100 km tiles. B) Mean percentage of forests averaged for 100 x100 km tiles. C) Statistical distribution of NDVI and type of land cover associated. D) Correlation between mean NDVI and mean percentage forest, averaged for 100 x 100 km tiles. The vertical black bars at 0 and 100 % correspond to the range of NDVI values for savannah (S) and non-mountainous forests (n-MF). Equation and R^2 are given only for non-mountainous forests (black dots).

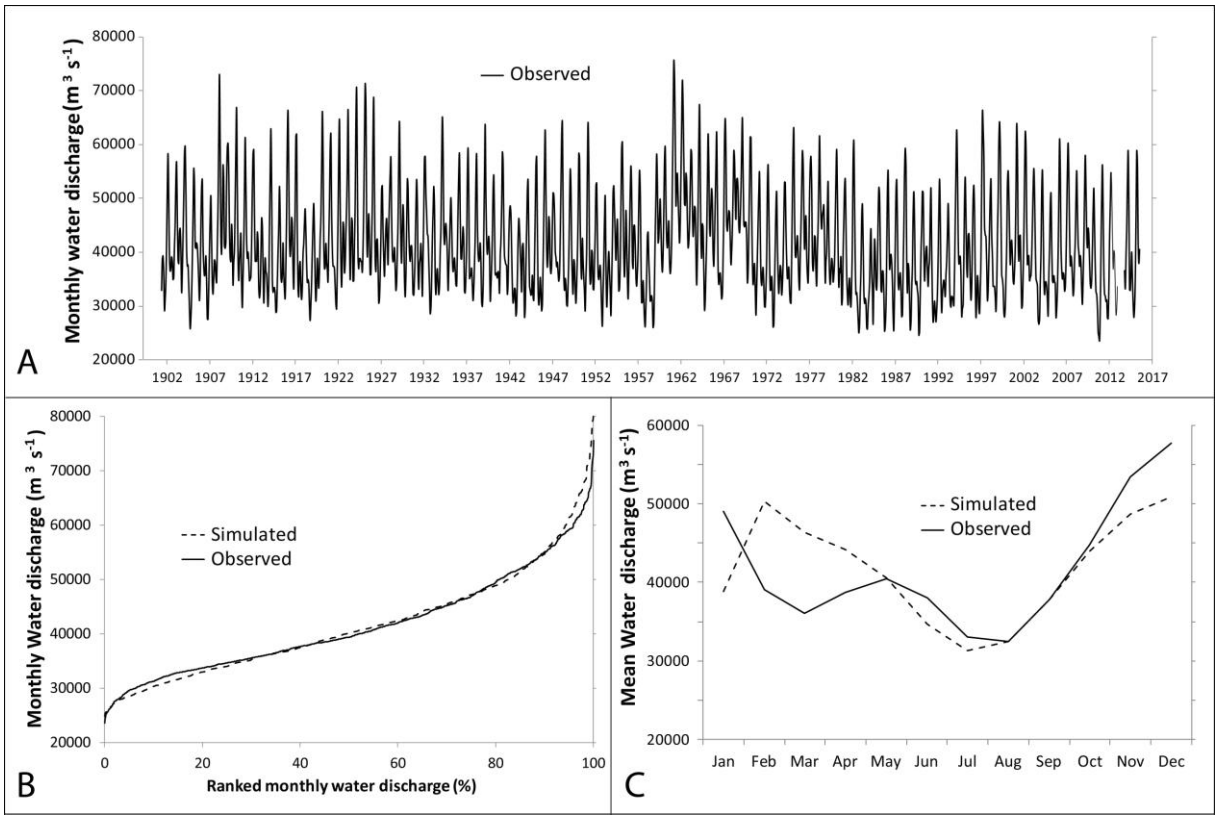

Figure 6: Calibration of simulated water discharge with present-day data. A) Observed, 114 years of monthly discharge data at the Brazzaville gauging station (Laraque et al., 2013a; HYBAM, 2016). B) Ranked monthly observed (solid line) and simulated (dashed line) water discharge. C) Monthly observed and simulated mean water discharge. These data highlight the capability of the HydroTrend model to simulate realistic discharges for the Congo River at Brazzaville.

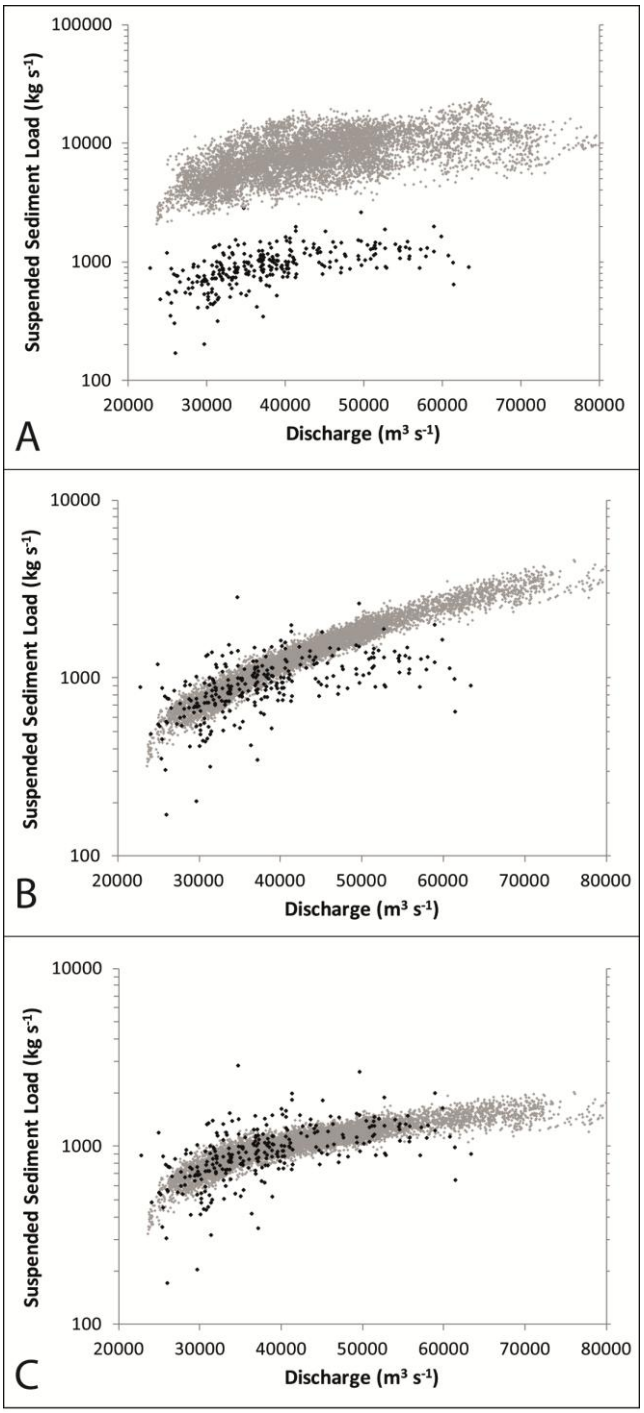

1035

1036 Figure 7: Calibration of simulated suspended sediment load with present-day observed data. The
1037 graphs A, B and C show the relation between suspended sediment load and water discharge. Observed
1038 data are represented as black dots; 20 years of daily simulated data are represented as grey dots. A)
1039 Simulations without trapping. B) Simulation including classic trapping (i.e. trapping by a lake) in the
1040 Cuvette Centrale. C) Simulation including classic and floodplain trapping when discharge exceed
1041 bankfull discharge (>33,000 m^3 s^{-1} for the best fit). To match simulated to observed data, sediment
1042 trapping by involving at least two distinct processes is needed.

1043

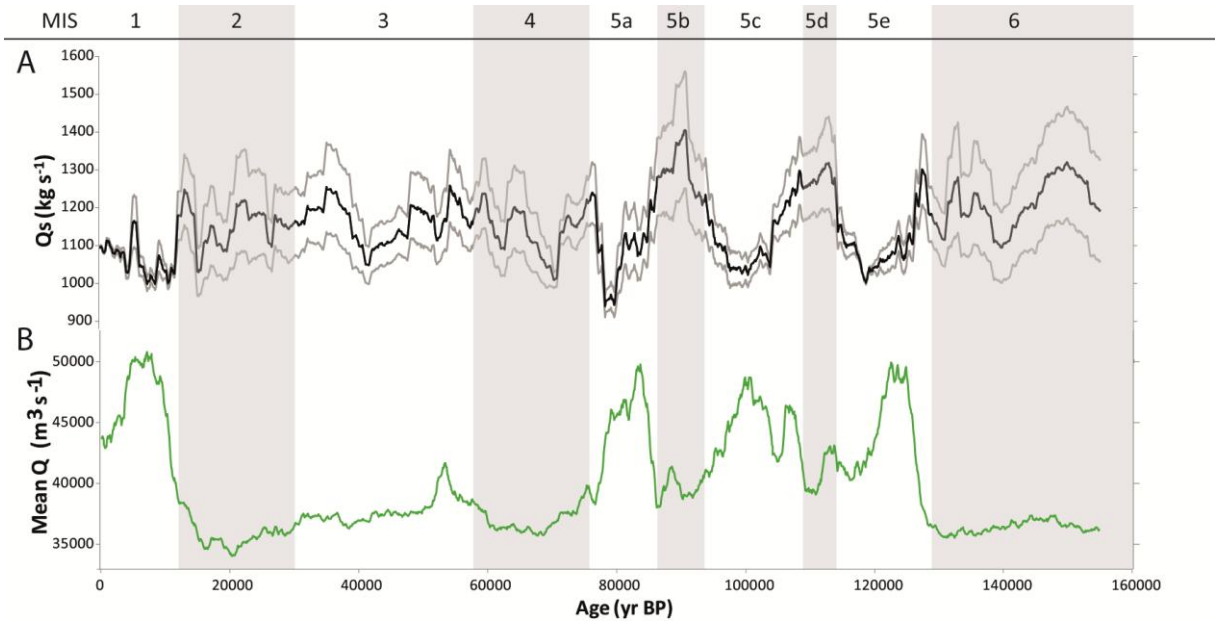

1044

1045 Figure 8: HydroTrend simulations of sediment load and water discharge over the last 155 ka. A)
1046 Simulated suspended sediment load evolution (Qs). The black curve corresponds to the mean sediment
1047 load, grey curves are the minimum and maximum with respect to vegetation index. B) Simulated
1048 water discharge. Curves A and B are running averages over 500 years of mean annual data simulated.

1049

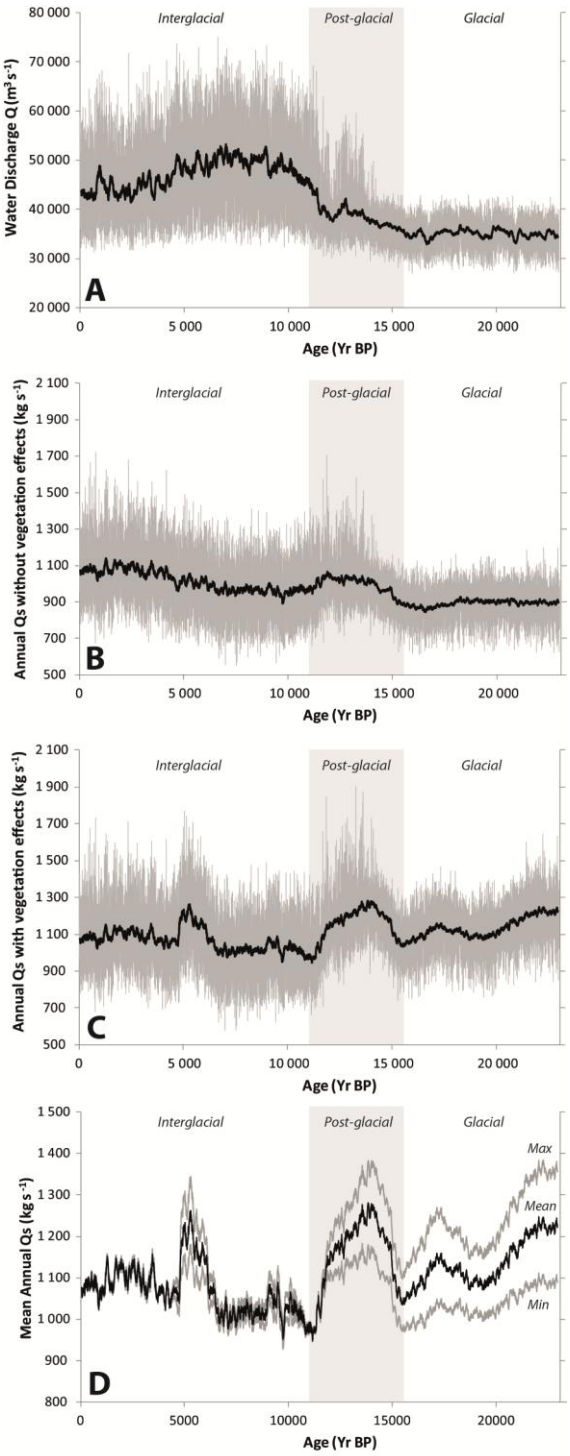

Figure 9: Water and suspended sediment simulation results focused over the last 23 ka. Gray curves represent annual data, while black curves are running means over 100 years. Three climatic periods (interglacial, post-glacial and glacial) are individualized by the light gray/white bands in background. A) Water discharge. B) Suspended sediment load without taking into account vegetation changes. C) Mean suspended sediment load taking into account vegetation changes. D) Running mean over 100 years of minimum (lower grey line), maximum (upper gray line) and mean (black line) suspended sediment load.

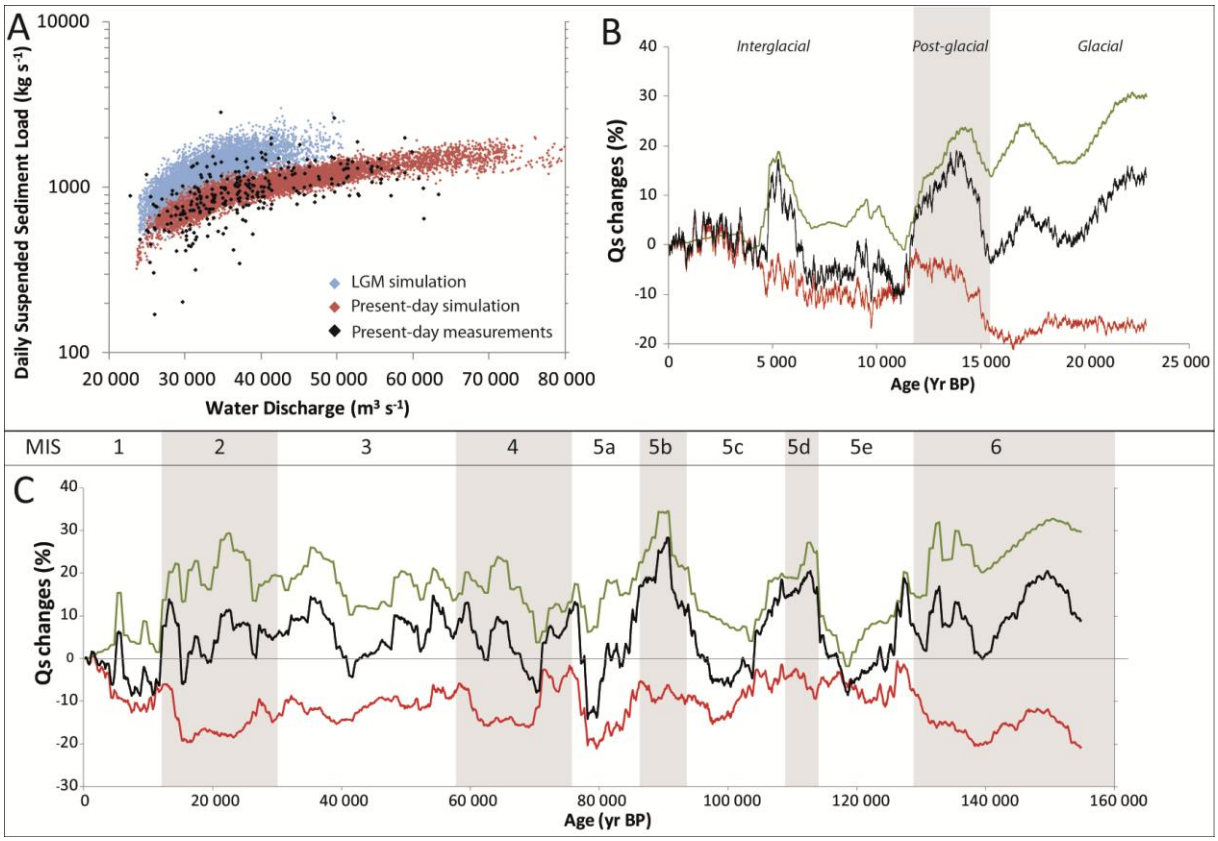

1058

1059 Figure 10: A) Relation between suspended sediment load and water discharge during present-day
1060 (observed data are represented with black triangles; 20 years of daily simulated data are represented
1061 with red triangles) and LGM conditions (20 years of daily simulation data are represented in blue). B)
1062 Deciphering the effect of only climate (without vegetation changes over time) (red curve) and only
1063 vegetation (green curve), and combined on mean suspended sediment load (black curve) for the last 23
1064 ka. On the background, the light gray period correspond to post-glacial stage. C) Deciphering the
1065 effect of climate and vegetation over the last 155 ka. The caption is the same as B except that light
1066 gray periods correspond to cold climatic stages.

1067

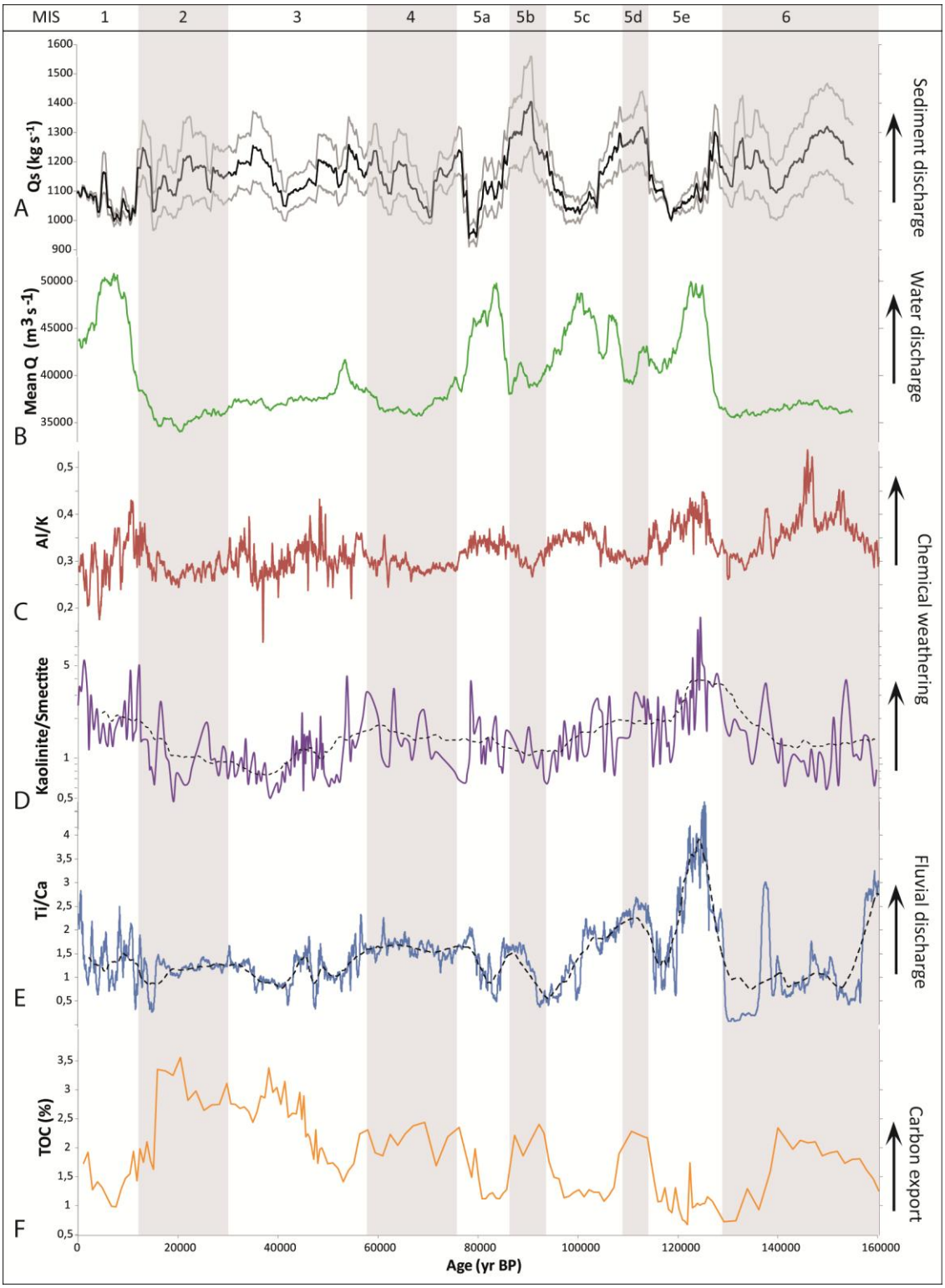

Figure 11: Comparisons of HydroTrend simulations with available offshore proxies related to sediment supply. A) and B) see caption in Fig. 8. C) Al/K semi-quantitative ratio measured with a XRF (Hatin et al., 2017). D) Log of Kaolinite/Smectite ratio (Sionneau et al., 2010). E) Ti/Ca semi-quantitative ratio measured with a XRF. F) Total Organic Carbon (TOC). Curves C to F were drawn from XRF measurements from core KZaï-02 (location in Figure 1). The dashed lines in D and E are running averages. In the background, the light gray periods correspond to cold climatic stages.

Table captions

Table 1: Values of parameters used in simulations.

Parameters	Value	Unit	Référence
Present-day yearly temperature	24.6	°C	Alsdorf et al., 2016
Standard deviation of yearly temperature	1.44	°C	Alsdorf et al., 2016
Present-day yearly precipitation	1630.1	mm	Alsdorf et al., 2016
Standard deviation of yearly precipitation	563	mm	Alsdorf et al., 2016
Precipitation mass balance coeficient	1		Syvitski et al., 1998
Distribition exponential	1.7		Syvitski et al., 1998
Distribution range	9		Syvitski et al., 1998
Constant annual baseflow	22000	$m^3.s^{-1}$	Alsdorf et al., 2016
Monthly Temperature	see Fig. 2D	°C	Hijmans et al., 2005
Monthly Precipitation	see Fig. 2D	mm	Hijmans et al., 2005
Lapse rate	6.4	$°C.km^{-1}$	Neumann, 1955
ELA start	4500	m	Osmaston and Harrison, 2005
Dry precipitation evaporation fraction	0		Syvitski et al., 1998
Average slope of the river bed delta	0.000183625		DEM
River lenght	4700	km	DEM
Volume of reservoirs	1000	km^3	DEM and our calibration
Altitude of reservoirs	290	m	DEM
Velocity coeficient (k)	0.56		Leopold and Maddock, 1953
Velocity exponent (m)	0.1		Leopold and Maddock, 1953
Width coeficient (a)	6.62		Leopold and Maddock, 1953
Width exponent (b)	0.61		Leopold and Maddock, 1953
Average velocity	1.23	$m^3.s^{-1}$	Laraque et al., 1995
Maximum groundwater storage	6.10^11	m^3	Cretaux et al., 2011; Becker et al., 2014
Minimum groundwater storage	10^11	m^3	Cretaux et al., 2011; Becker et al., 2014
Initial groundwater storage	3.5.10^11	m^3	Cretaux et al., 2011; Becker et al., 2014
Groundwater coeficient	15000	$m^3.s^{-1}$	Cretaux et al., 2011; Becker et al., 2014
Groundwater exponent	1.4		Cretaux et al., 2011; Becker et al., 2014
Saturated hydraulic conductivity	315	$mm.day^{-1}$	Bear, 1972 and our calibration
Latitude of the outlet	15.3 N		DEM
Longitude of the outlet	4.283 W		DEM
Lithology factor (L)	1		Syvitski and Milliman, 2007
Anthropogenic factor	1		Syvitski and Milliman, 2007
Landcover factor	0.6444-0.7325		our calibration (min-max)
Bankfull discharge	33000	$m^3.s^{-1}$	our calibration
Altitude of bankfull discharge	350	m	DEM